Journal of Human Evolution 108 (2017) 176–198

Contents lists available at ScienceDirect

Journal of Human Evolution

journal homepage: www.elsevier.com/locate/jhevol

# Catarrhine hallucal metatarsals from the early Miocene site of Songhor, Kenya

Biren A. Patel [a, b, *], Gabriel S. Yapuncich [c], Cassandra Tran [b], Isaiah O. Nengo [d]

[a] Department of Integrative Anatomical Sciences, Keck School of Medicine, University of Southern California, Los Angeles, CA 90033, USA
[b] Human and Evolutionary Biology Section, Department of Biological Sciences, University of Southern California, Los Angeles, CA 90089, USA
[c] Department of Evolutionary Anthropology, Duke University, Durham, NC 27708, USA
[d] Department of Anthropology, De Anza College, Cupertino, CA 95104, USA

ARTICLE INFO

*Article history:*
Received 27 September 2016
Accepted 20 March 2017

*Keywords:*
Grasping foot
Hallux
Hominoid
*Dendropithecus*
*Proconsul*
*Rangwapithecus*

ABSTRACT

Songhor is an early Miocene fossil locality in Kenya known for its diverse primate assemblage that includes catarrhine species belonging to the genera *Kalepithecus*, *Limnopithecus*, *Dendropithecus*, *Rangwapithecus*, and *Proconsul*. Expeditions to Songhor since the 1930s have recovered unassociated catarrhine postcranial remains from both the fore- and hindlimbs, including multiple elements from the feet. In this study, we describe KNM-SO 31233, a complete left hallucal metatarsal (Mt1), along with several other fragmentary Mt1 specimens (KNM-SO 1080, 5129, 5141, 22235). These fossils were compared to extant catarrhines and platyrrhines, as well as available fossil Miocene catarrhine Mt1s. Morphometric data were obtained from 3D surface renderings and subjected to a number of analyses to assess their phenetic affinity with the comparative sample, make predictions of body mass, and to infer their functional morphology. The size and shape of the Songhor Mt1s are diverse, exhibiting a large robust morph (KNM-SO 5141) similar in size but not in shape to extant African apes, medium-sized morphs (KNM-SO 1080, 5129 and 22235), and a smaller, slender one (KNM-SO 31233) that has a shape resembling arboreal quadrupedal leaping monkeys and suspensory atelines and hylobatids. KNM-SO 31233 is unlike other known fossil Mt1s, and in general, none of the Songhor Mt1s resembled any single extant anthropoid clade or species. The morpho-functional diversity of Songhor Mt1s is consistent with an extensive morphological and phylogenetic catarrhine diversity in the early part of the Miocene epoch.



## 1. Introduction

Songhor is one of a number of fossil sites located around the slopes of the Miocene Tinderet Volcano in the western part of Kenya. It has been dated to ~19–20 Ma (Bishop et al., 1969). Songhor was discovered by Louis Leakey and Donald MacInnes in 1931–1932 (MacInnes, 1943) and subsequent surveys and excavations were organized by Leakey in 1948 and 1966, Andrews in 1972 (Pickford and Andrews, 1981), and by one of the authors (ION) in 1989–1990, 1996, 1998 and 2013–2014 (Nengo and Rae, 1992; Cote and Nengo, 2007). Songhor has produced a number of important fossil primates that are both taxonomically and ecomorphologically diverse. It is generally accepted that the dentognathic primate remains discovered at Songhor can be attributed to five non-cercopithecoid catarrhine species: *Kalepithecus songhorensis*, *Limnopithecus evansi*, *Dendropithecus macinnesi*, *Rangwapithecus gordoni*, and *Proconsul major*[1] (Andrews, 1978; Harrison, 1982, 1988, 2002, 2010; Pickford, 1986; Nengo and Rae, 1992; Cote et al., 2016). Both *K. songhorensis* and *R. gordoni* are unique to Songhor (Harrison, 1982, 2002; Hill et al., 2013) with *K. songhorensis* occurring less frequently (R. Jansma, pers. comm.). Both *D. macinnesi* and *P. major* are found at other contemporaneous sites in Kenya and Uganda (e.g., Le Gros Clark and Thomas, 1951; Andrews, 1978; Harrison, 1982, 2002; Pickford et al., 2009). While

[1] Some authors have made arguments that the craniodental and postcranial specimens from Kenya (including Songhor) and Uganda attributed to *Proconsul major* should be referred to as *Ugandapithecus major* (Senut et al., 2000; Pickford et al., 2009). In this study, we keep to the original name *P. major* following Harrison and Andrews (2009, see also MacLatchy and Rossie, 2005). Also, we follow McNulty et al. (2015) in splitting *Proconsul* sensu lato species into two genera, *Proconsul* and *Ekembo*.

* Corresponding author.
*E-mail address:* birenpat@usc.edu (B.A. Patel).

http://dx.doi.org/10.1016/j.jhevol.2017.03.013
0047-2484/

there are several species of *Limnopithecus* also found at a number of sites in Kenya and Uganda, *L. evansi* is found only at Songhor and the Mteitei Valley localities (Harrison, 2010; Cote et al., 2016).

Reconstructions of the locomotor behaviors of the Songhor primates, and in general almost all early Miocene catarrhines, have been difficult. This is largely because the postcranial specimens (>140 specimens catalogued as of 2016) are fragmentary and unassociated. Moreover, the postcranial remains have been difficult to assign to any single species because many Songhor primates overlap in size. For postcranial material recovered before the late 1980s, many assignments of specimens to any particular Songhor species were tentative and often used open nomenclature ('cf.'; e.g., Harrison, 1982) which is a common practice. Of these, the most confident assignments are likely those made to *P. major*, which is significantly larger than the other primates at Songhor (Rafferty et al., 1995; see body mass estimates summarized in Table 15.1 in Fleagle, 2013). Moreover, the majority of the postcranial fossils from Songhor discovered in the last 20 years have yet to be formally described. The few exceptions include one study on the bones of the elbow complex (which were tentatively attributed to *R. gordoni* by Gebo et al. [2009]) and some preliminary work on tarsals (Nengo and Rae, 1992) and capitates (Wurthrich et al., 2016).

In general, what little we know of the postcranial skeleton of the five Songhor catarrhines actually comes from other nearby localities in Kenya and Uganda. For example, elements from the elbow, hip and ankle attributed to *P. major* have been described in detail from Napak (Rafferty et al., 1995; Gommery et al., 1998, 2002). From these specimens, this species has been reconstructed to be a quadruped that frequented the ground and was capable of vertical climbing. Many parts of the skeleton of *D. macinnesi* are also known from multiple individuals recovered at Rusinga Island (Le Gros Clark and Thomas, 1951). Most researchers agree that its postcranial skeleton was likely adapted for above-branch quadrupedalism with frequent bouts of forelimb suspension and leaping, and it may have also been capable of postural suspension with the foot (e.g., Le Gros Clark and Thomas, 1951; Harrison, 1982; Fleagle, 1983; Rose et al., 1992; Rose, 1996). To date, we are unaware of any postcranial specimens that have been definitely attributed to *Limnopithecus* and *Kalepithecus* (Harrison, 1982, 2002; Rose et al., 1992), and those assigned to *Rangwapithecus* have been attributed to this taxon only tentatively (Harrison, 1982; Gebo et al., 2009). Thus, not only having more postcranial specimens, but also those that can possibly be better assigned to a species, may improve our understanding of the locomotor biology of these early Miocene primates. Moreover, new postcranial fossils may help us better comprehend the complexity of catarrhine postcranial evolution in general (e.g., Rose, 1983).

In this study, we describe one complete and four fragmentary hallucal metatarsals (Mt1) from Songhor (Fig. 1). The hallux has played an important role in primate evolution (e.g., Morton, 1924; Szalay and Dagosto, 1988; Lewis, 1989; Patel et al., 2012) and a number of important variables, including body size, substrate preference, and positional behavior can determine its morphology and how it is used as a grasping organ (e.g., Goodenberger et al., 2015). An abducted prehensile hallux is an important organ for small to medium-sized primates, including anthropoids, because it can play an essential role in pedal grasping that is necessary to maintain stability during locomotion in a complex three-dimensional arboreal environment composed of substrates of varying orientations and diameters (Martin, 1990). For those non-human primates of relatively larger size and adapted to more terrestrial habitats (e.g., African apes and some Old World monkeys), an abducted hallux is likely used more as a strut to supplement weight support when walking on the ground and/or aid in climbing vertical tree trunks (Meldrum, 1991; Vereecke et al., 2003). Both functional roles likely characterize how the hallux was used by different early Miocene catarrhines including those found at Songhor. Of the four specimens described here, KNM-SO 22235 and 31233 were recovered in 1989 and 1996, respectively, from the screen-washing of sediments obtained during excavation. Specimens KNM-SO 1080, 5129 and 5141 were collected during earlier field seasons. KNM-SO 1080 was found in 1972, and SO 5129 and 5141 in 1966. While these last three Mt1 specimens have been previously discussed by Harrison (1982) and Langdon (1984, 1986), none has been formally described in detail and thus they are given a more thorough treatment in this study. Harrison (1982) assigned both KNM-SO 1080 and 5129 to cf. *R. gordoni*, and identified KNM-SO 5141 as *P. major* based on their respective sizes.

## 2. Materials and methods

### 2.1. Materials

The sample of extant and fossil Mt1s used in this study and/or referred to in this manuscript are housed in the following institutions: AMNH, American Museum of Natural History (New York, NY); CPRC, Caribbean Primate Research Center (San Juan, PR); DPC, Duke Lemur Center's Division of Fossil Primates (Durham, NC); GSP, Geological Survey of Pakistan (Quetta, Pakistan); KNM, National Museums of Kenya (Nairobi, Kenya); LACM, Los Angeles County Museum of Natural History (Los Angeles, CA); MCZ, Harvard University's Museum of Comparative Zoology (Cambridge, MA); NMNH, National Museum of Natural History (Paris, France); RMCA, Royal Museum for Central Africa (Tervuren, Belgium); SBU, Department of Anatomical Sciences of Stony Brook University (Stony Brook, NY); USNM, Smithsonian Institution's National Museum of Natural History (Washington, DC); YPM, Yale Peabody Museum (New Haven, CT).

For the Songhor Mt1 specimens, original fossils as well as 3D virtual surface models were studied to make observations and obtain measurements as detailed below. The only exception was KNM-SO 5129, for which observations and measurements were taken only on the original fossil specimen.

The extant comparative sample is comprised of 404 Mt1s and includes hominoids, cercopithecoids and non-callitrichine platyrrhines (Table 1). Only extant specimens with known sex were included. The other fossil catarrhine Mt1s examined here (either original fossils or casts) include complete and fragmentary specimens that have been attributed to: *Aegyptopithecus zeuxis* (DPC 13318 [Patel et al., 2012]; YPM 25806 [Conroy, 1976]); *Afropithecus turkanensis* (KNM-WK 18119 [Leakey et al., 1988]); *Catopithecus browni* (DPC 20939 [Patel et al., 2012]); *Epipliopithecus vindobonensis* (Individuals 1, 2 and 3 [Zapfe, 1958, 1960]); *Nacholapithecus kerioi* (KNM-BG 35250-AJ [Ishida et al., 2004]); *Ekembo heseloni* (KNM-RU 2036 [Napier and Davis, 1959]; KNM-KPS III and VIII [Walker and Teaford, 1988]); and *Ekembo nyanzae* (KNM-RU 5872 [Walker and Pickford, 1983]; KNM-RU 17392 [Rose et al., 1996]). Additional metric and qualitative data for the following fossils were obtained from the literature because the authors were not able to study these specimens directly: *N. kerioi* (KNM-BG 17814 [referred to as *Kenyapithecus* in Rose et al., 1996]); *Proconsul* cf. *africanus* (KNM-CA 1865, 1889, 2236, 2239 [Harrison, 1982]); *E. heseloni* (KNM-RU 15074 [Rose et al., 1996]); and *Sivapithecus parvada* (GSP 14046 [Pilbeam et al., 1980; Rose et al., 1996]). Measurements for the fossil specimens are presented in Table 2.

### 2.2. Mt1 measurements

Three-dimensional (3D) virtual surface renderings of Mt1s were created from computed tomography scans (CT), micro-CT scans

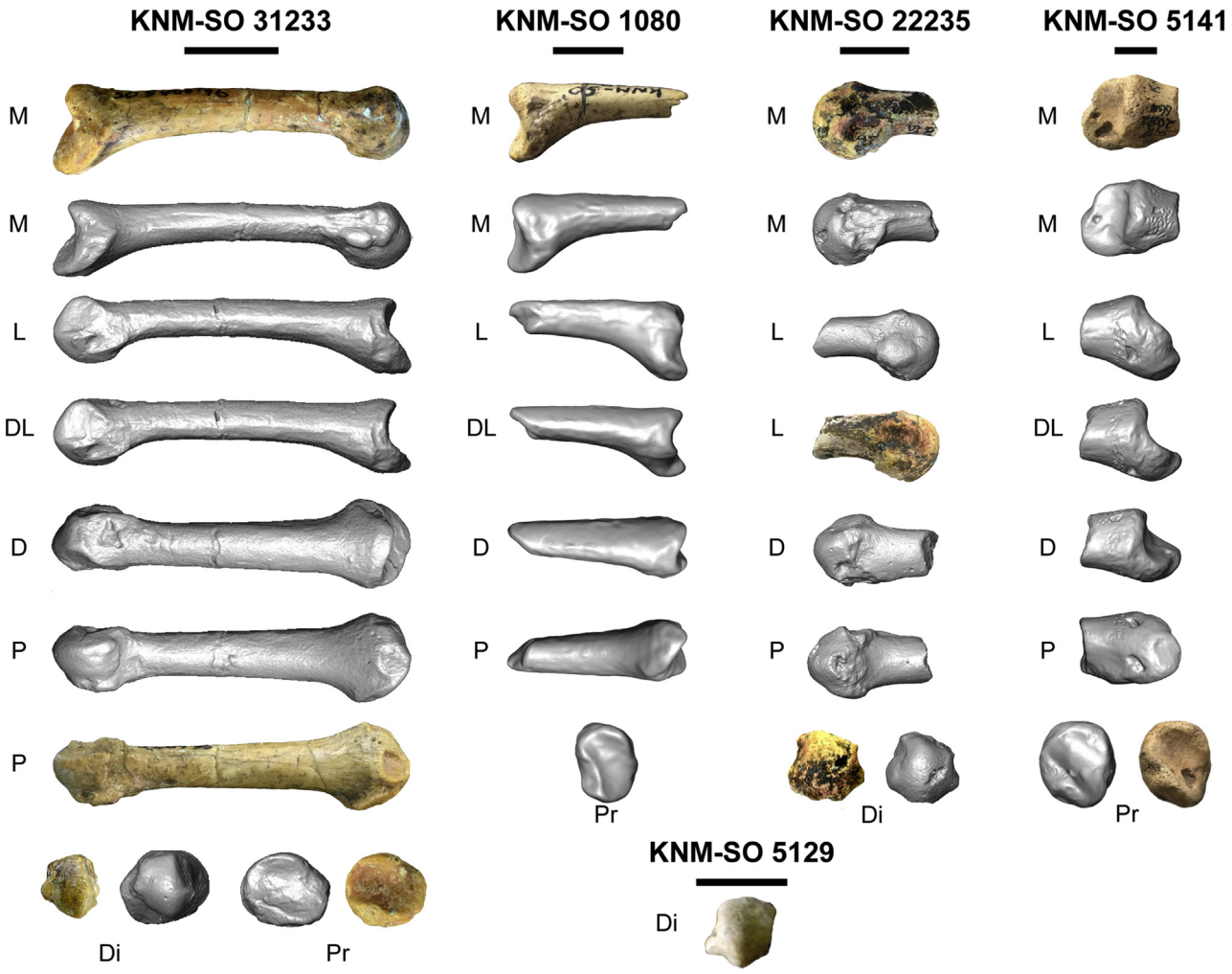


**Figure 1.** Photographs and virtual reconstructions of Songhor fossil Mt1s. M, medial; L, lateral; DL, dorsolateral; D, dorsal; P, plantar; Pr, proximal; Di, distal. Scale bars equal 1 cm. Specimens KNM-SO 31233, 1080, and 5141 are from the left side and KNM-SO 22235 and 5129 are from the right side. The virtual reconstructions were derived from either laser scans of the original fossils or from microCT scans of casts of the original fossils. 3D Mt1 models are available on the www.morphosource.org website.

(μCT), or laser scans. The majority of the CT scan data were obtained at Stony Brook University Medical Center using a GE Lightspeed VCT CT scanner (setting: 120 kV, 250 mA, 1 mm slice thickness, 0.187 mm slice interval, 'Bone Plus' reconstruction protocol). The acquisition of additional CT data to create 3D renderings are provided in Jashashvili et al. (2015). The μCT scan data were obtained at Stony Brook University's Department of Biomedical Engineering using a SCANCO Medical vivaCT 75 preclinical scanner (setting: isometric voxel resolution of 20–80 μm) or at the University of Southern California's Molecular Imaging Center using either a SCANCO μCT 50 specimen scanner or GE Phoenix Nanotom M scanner (settings: isometric voxel resolution of 15–50 μm). The CT and μCT scan data were segmented on unfiltered 16-bit DICOM (.dcm) images using the LabelField function in Amira v.5.6 or Avizo v.7.0 software using a combination of automated and slice-by-slice manual thresholding techniques. Surface renderings were created using the SurfaceGen tool (with unconstrained smoothing and compactify options) and saved as POLYGON mesh files (.ply). Laser scans were obtained with a NextEngine 3D laser scanner using a resolution of >10,000 points per square inch; 6–9 scans were taken at different positions and then merged using ScanStudio HD PRO software and saved as .ply files. Any scanning defects in the mesh surface models created from any of the scanning modalities were corrected using Geomagic Studio v.12 software.

All measurements were taken on left side elements. If the original specimen was from the right side, it was mirror imaged in Amira software using the Transform Editor tool to create its antimere. Prior to taking measurements, each digital Mt1 was reoriented in Amira software following a standardized orientation protocol such that: 1) the dorsal surface of the diaphysis in medial view (XY) approximated the parallel along the horizontal (Fig. 2A); 2) a line connecting the centers of the proximal and distal articular surfaces in dorsal view (XZ) was parallel along the horizontal (Fig. 2B); and 3) the deepest parts of the distal head's sesamoid gutters (facets) plantar to the epicondyles approximated a straight line that ran perpendicular to the horizontal in distal view (YZ) (Fig. 2C). Accordingly, all dorsoplantar and mediolateral measurements are referenced to the distal head of the specimen and not necessarily a true anatomical or functional orientation (which can vary widely depending on overall pedal form and function; Goodenberger et al., 2015; Jashashvili et al., 2015). The initial reorientation of specimens was facilitated using the AlignPrincipalAxes function, and this was followed by minor manual movements using the Transform Editor tool, both in Amira software.

All 3D linear measurements (in mm) were obtained using Amira software. These include the bone's maximum length and interarticular length (IAL), and the dorsoplantar height (DPH) and mediolateral width (MLW) dimensions taken at five locations

**Table 1**
Means and standard deviations of Mt1 variables for the extant sample.[a,b]

| Taxon | *n* | | IAL | B- DPH | B-MLW | 25%-DPH | 25%-MLW | 50%-DPH | 50%-MLW | 75%-DPH | 75%-MLW | H- DPH | H-MLW | GMean (11) | GMean (Di) | CunM Area | PAA[c] |
|---|---|---|---|---|---|---|---|---|---|---|---|---|---|---|---|---|---|
| *Allenopithecus nigroviridis* | 2 | X | 27.23 | 7.26 | 6.54 | 4.07 | 4.77 | 3.10 | 3.64 | 2.65 | 3.74 | 3.97 | 5.89 | 5.13 | 3.90 | 25.02 | 96.38 |
| | | SD | 4.11 | 0.83 | 0.98 | 0.64 | 0.88 | 0.26 | 1.03 | 0.30 | 0.86 | 0.60 | 0.83 | 0.82 | 0.62 | 6.25 | – |
| *Alouatta belzebul* | 1 | X | 28.73 | 8.25 | 9.64 | 5.55 | 6.30 | 4.14 | 4.76 | 4.41 | 5.33 | 7.75 | 6.96 | 7.01 | 5.97 | 41.92 | – |
| *Alouatta caraya* | 2 | X | 29.49 | 8.42 | 8.43 | 5.62 | 6.08 | 4.16 | 4.76 | 4.22 | 5.03 | 6.33 | 7.65 | 6.80 | 5.66 | 34.42 | – |
| | | SD | 3.22 | 0.45 | 0.34 | 0.26 | 0.21 | 0.23 | 0.13 | 0.28 | 0.01 | 0.71 | 0.39 | 0.37 | 0.33 | 5.68 | – |
| *Alouatta guariba* | 1 | X | 23.88 | 7.95 | 7.91 | 5.16 | 5.82 | 4.09 | 4.29 | 4.10 | 4.83 | 5.64 | 6.28 | 6.24 | 5.15 | 30.50 | – |
| *Alouatta palliata* | 1 | X | 27.48 | 8.60 | 8.17 | 5.65 | 5.43 | 4.06 | 4.11 | 4.36 | 5.47 | 7.13 | 7.59 | 6.73 | 5.99 | 32.02 | – |
| *Alouatta pigra* | 1 | X | 29.99 | 8.50 | 8.35 | 6.06 | 6.39 | 4.29 | 5.10 | 4.49 | 5.40 | 6.85 | 7.67 | 7.10 | 5.97 | 35.01 | – |
| *Alouatta seniculus* | 9 | X | 30.08 | 8.50 | 8.43 | 5.51 | 5.65 | 4.19 | 4.43 | 4.26 | 4.98 | 6.52 | 7.15 | 6.70 | 5.60 | 35.03 | 98.97 |
| | | SD | 1.61 | 0.45 | 0.57 | 0.33 | 0.33 | 0.25 | 0.41 | 0.38 | 0.25 | 0.41 | 0.46 | 0.27 | 0.25 | 2.82 | 4.24 |
| *Aotus azarae* | 8 | X | 19.08 | 4.43 | 4.14 | 2.62 | 2.95 | 2.16 | 2.26 | 2.13 | 2.29 | 3.49 | 3.45 | 3.43 | 2.77 | 7.72 | 109.08 |
| | | SD | 0.63 | 0.23 | 0.18 | 0.08 | 0.13 | 0.07 | 0.13 | 0.14 | 0.11 | 0.23 | 0.21 | 0.12 | 0.15 | 1.16 | 4.54 |
| *Aotus infulatus* | 1 | X | 17.05 | 4.27 | 3.82 | 2.55 | 2.78 | 1.93 | 2.13 | 2.01 | 2.28 | 3.42 | 3.28 | 3.24 | 2.68 | 5.63 | – |
| *Ateles belzebuth* | 3 | X | 33.23 | 9.38 | 9.06 | 5.80 | 6.15 | 4.38 | 4.70 | 4.48 | 5.26 | 7.28 | 7.36 | 7.18 | 5.96 | 47.08 | 104.58 |
| | | SD | 4.26 | 1.15 | 0.49 | 0.07 | 0.85 | 0.52 | 0.48 | 0.58 | 0.66 | 0.51 | 0.75 | 0.69 | 0.61 | 6.66 | 6.00 |
| *Ateles fusciceps* | 2 | X | 35.35 | 10.24 | 8.85 | 5.82 | 5.98 | 4.23 | 4.90 | 4.49 | 6.26 | 8.21 | 8.01 | 7.49 | 6.54 | 52.66 | 99.42 |
| | | SD | 1.40 | 0.75 | 0.04 | 0.88 | 0.47 | 0.67 | 0.66 | 0.01 | 0.66 | 1.77 | 0.16 | 0.64 | 0.50 | 6.91 | – |
| *Ateles geoffroyi* | 1 | X | 34.07 | 9.15 | 9.65 | 5.66 | 6.20 | 4.27 | 5.70 | 4.18 | 5.55 | 7.27 | 7.51 | 7.32 | 5.97 | 46.79 | 99.98 |
| *Ateles marginatus* | 4 | X | 35.15 | 9.28 | 8.94 | 5.67 | 5.88 | 4.21 | 4.63 | 4.93 | 5.43 | 7.57 | 7.55 | 7.24 | 6.25 | 46.22 | – |
| | | SD | 2.19 | 0.60 | 0.24 | 0.32 | 0.42 | 0.34 | 0.27 | 0.36 | 0.63 | 0.34 | 0.37 | 0.38 | 0.38 | 6.61 | – |
| *Callicebus donacophilus* | 5 | X | 16.59 | 4.60 | 3.50 | 2.70 | 2.83 | 1.96 | 2.02 | 1.97 | 1.98 | 3.22 | 3.43 | 3.19 | 2.56 | 9.05 | – |
| | | SD | 0.71 | 0.16 | 0.14 | 0.09 | 0.12 | 0.06 | 0.05 | 0.07 | 0.06 | 0.09 | 0.15 | 0.04 | 0.05 | 0.57 | – |
| *Cebus albifrons* | 8 | X | 27.89 | 7.83 | 6.95 | 4.78 | 4.77 | 3.55 | 3.87 | 3.61 | 4.35 | 5.79 | 6.68 | 5.87 | 4.96 | 28.97 | – |
| | | SD | 1.99 | 0.57 | 0.42 | 0.38 | 0.41 | 0.28 | 0.20 | 0.25 | 0.26 | 0.70 | 0.49 | 0.29 | 0.30 | 3.61 | – |
| *Cebus capucinus* | 3 | X | 29.13 | 7.62 | 7.14 | 4.76 | 4.72 | 3.65 | 4.04 | 3.51 | 4.38 | 5.52 | 6.63 | 5.88 | 4.87 | 27.46 | – |
| | | SD | 2.38 | 0.50 | 0.23 | 0.32 | 0.13 | 0.32 | 0.33 | 0.32 | 0.12 | 0.45 | 0.20 | 0.28 | 0.26 | 1.92 | – |
| *Cebus olivaceus* | 5 | X | 28.31 | 7.63 | 6.25 | 4.28 | 4.51 | 3.47 | 3.78 | 3.31 | 3.88 | 5.64 | 6.24 | 5.55 | 4.61 | 27.80 | – |
| | | SD | 0.88 | 0.34 | 0.64 | 0.31 | 0.35 | 0.22 | 0.20 | 0.30 | 0.19 | 0.16 | 0.45 | 0.26 | 0.21 | 3.28 | – |
| *Cercocebus agilis* | 1 | X | 37.61 | 9.93 | 10.35 | 6.78 | 7.02 | 4.93 | 5.65 | 4.16 | 5.43 | 6.77 | 7.69 | 7.75 | 5.86 | 58.83 | 96.97 |
| *Cercocebus galeritus* | 1 | X | 37.91 | 10.96 | 10.19 | 7.01 | 7.18 | 4.96 | 5.81 | 4.44 | 6.02 | 7.15 | 8.93 | 8.15 | 6.43 | 53.72 | 99.84 |
| *Cercopithecus alborgularis* | 1 | X | 28.49 | 8.77 | 7.47 | 5.59 | 5.95 | 3.84 | 4.58 | 3.71 | 4.74 | 5.92 | 6.85 | 6.43 | 5.17 | 33.02 | – |
| *Cercopithecus ascanius* | 3 | X | 28.61 | 6.72 | 7.42 | 4.59 | 5.14 | 3.38 | 3.99 | 3.20 | 3.92 | 6.36 | 5.39 | 5.67 | 4.55 | 26.79 | – |
| | | SD | 1.06 | 0.20 | 0.67 | 0.31 | 0.44 | 0.15 | 0.27 | 0.14 | 0.08 | 0.48 | 0.19 | 0.23 | 0.13 | 4.54 | – |
| *Cercopithecus lowei* | 1 | X | 22.99 | 6.13 | 5.55 | 3.52 | 3.65 | 2.69 | 2.76 | 2.60 | 3.08 | 4.16 | 5.17 | 4.43 | 3.62 | 18.75 | – |
| *Cercopithecus mitis* | 7 | X | 28.96 | 7.83 | 7.54 | 4.81 | 5.29 | 3.56 | 4.10 | 3.46 | 4.15 | 5.45 | 6.80 | 5.95 | 4.80 | 33.27 | – |
| | | SD | 2.78 | 0.82 | 0.75 | 0.71 | 0.56 | 0.44 | 0.51 | 0.43 | 0.63 | 0.57 | 0.68 | 0.64 | 0.54 | 5.78 | – |
| *Cercopithecus mona* | 2 | X | 27.31 | 7.60 | 7.03 | 4.72 | 4.75 | 3.56 | 3.84 | 3.23 | 4.19 | 4.76 | 6.24 | 5.62 | 4.47 | 26.22 | 105.04 |
| | | SD | 1.93 | 1.18 | 0.37 | 0.78 | 0.62 | 0.47 | 0.44 | 0.25 | 0.34 | 0.30 | 0.05 | 0.53 | 0.24 | 5.50 | – |
| *Cercopithecus neglectus* | 1 | X | 31.77 | 8.62 | 7.43 | 5.40 | 5.44 | 3.88 | 4.14 | 3.57 | 4.53 | 6.40 | 7.60 | 6.41 | 5.30 | 35.82 | 97.36 |
| *Chiropotes albinasus* | 1 | X | 25.00 | 6.40 | 5.73 | 3.44 | 3.43 | 2.52 | 3.13 | 2.69 | 3.25 | 4.85 | 5.32 | 4.59 | 3.88 | 22.26 | – |
| *Chiropotes satanas* | 2 | X | 23.17 | 6.08 | 5.23 | 3.38 | 3.48 | 2.58 | 2.89 | 2.62 | 3.06 | 4.98 | 5.00 | 4.43 | 3.76 | 20.64 | 102.52 |
| | | SD | 2.23 | 0.95 | 0.83 | 0.45 | 0.24 | 0.31 | 0.30 | 0.10 | 0.10 | 0.57 | 0.18 | 0.43 | 0.21 | 7.87 | 1.23 |
| *Chlorocebus aethiops* | 16 | X | 25.49 | 6.88 | 6.37 | 4.26 | 4.76 | 3.31 | 3.72 | 3.09 | 4.06 | 4.88 | 6.04 | 5.35 | 4.38 | 24.43 | 98.56 |
| | | SD | 2.88 | 0.64 | 0.63 | 0.50 | 0.51 | 0.42 | 0.44 | 0.33 | 0.50 | 0.50 | 0.58 | 0.53 | 0.43 | 4.73 | 3.70 |
| *Colobus angolensis* | 3 | X | 35.60 | 9.39 | 7.74 | 5.56 | 5.63 | 4.52 | 4.68 | 4.00 | 4.52 | 6.03 | 6.75 | 6.71 | 5.21 | 39.48 | – |
| | | SD | 1.75 | 0.25 | 0.33 | 0.43 | 0.32 | 0.55 | 0.10 | 0.20 | 0.26 | 0.12 | 0.30 | 0.13 | 0.19 | 2.95 | – |
| *Colobus guereza* | 10 | X | 32.06 | 8.70 | 7.43 | 5.02 | 5.01 | 3.75 | 4.27 | 3.77 | 4.26 | 6.65 | 6.53 | 6.26 | 5.14 | 32.70 | 97.36 |
| | | SD | 2.44 | 0.34 | 0.47 | 0.39 | 0.44 | 0.29 | 0.30 | 0.31 | 0.22 | 0.50 | 0.48 | 0.36 | 0.33 | 4.47 | 2.42 |
| *Colobus polykomos* | 6 | X | 32.88 | 9.22 | 7.35 | 5.77 | 5.22 | 4.02 | 4.50 | 3.94 | 4.52 | 6.88 | 6.84 | 6.59 | 5.38 | 35.71 | 89.67 |
| | | SD | 1.07 | 0.46 | 0.29 | 0.39 | 0.34 | 0.20 | 0.34 | 0.28 | 0.35 | 0.71 | 0.49 | 0.36 | 0.41 | 3.78 | – |
| *Erythrocebus patas* | 19 | X | 28.35 | 8.20 | 7.09 | 5.02 | 5.75 | 3.61 | 4.41 | 3.40 | 4.70 | 5.73 | 6.67 | 6.12 | 4.96 | 28.79 | 93.01 |
| | | SD | 3.16 | 0.87 | 0.87 | 0.53 | 0.68 | 0.39 | 0.55 | 0.40 | 0.58 | 0.63 | 0.73 | 0.62 | 0.50 | 5.78 | – |
| *Gorilla beringei* | 7 | X | 55.63 | 26.11 | 21.59 | 19.84 | 16.03 | 12.36 | 14.20 | 12.80 | 18.96 | 15.56 | 18.34 | 19.02 | 16.19 | 284.67 | – |
| | | SD | 5.98 | 2.69 | 4.56 | 2.50 | 3.90 | 1.83 | 2.59 | 3.68 | 3.12 | 2.77 | 3.24 | 3.10 | 3.15 | 77.18 | – |
| *Gorilla gorilla* | 24 | X | 59.36 | 27.23 | 21.88 | 20.92 | 16.18 | 12.15 | 13.95 | 12.65 | 19.91 | 15.68 | 19.49 | 19.47 | 16.62 | 309.16 | 95.50 |

(*continued on next page*)

**Table 1** (*continued*)

| Taxon | *n* | | IAL | B- DPH | B-MLW | 25%-DPH | 25%-MLW | 50%-DPH | 50%-MLW | 75%-DPH | 75%-MLW | H- DPH | H-MLW | GMean (11) | GMean (Di) | CunM Area | PAA[c] |
|---|---|---|---|---|---|---|---|---|---|---|---|---|---|---|---|---|---|
| | | SD | 5.47 | 2.95 | 2.59 | 3.03 | 2.51 | 1.65 | 1.93 | 1.59 | 2.42 | 2.04 | 1.91 | 2.08 | 1.66 | 62.79 | – |
| *Hoolock hoolock* | 3 | X | 37.49 | 10.95 | 9.05 | 6.54 | 6.09 | 4.82 | 5.18 | 4.68 | 6.39 | 7.21 | 8.46 | 7.82 | 6.53 | 50.88 | 96.02 |
| | | SD | 1.22 | 0.21 | 0.17 | 0.14 | 0.17 | 0.06 | 0.15 | 0.24 | 0.55 | 0.13 | 0.43 | 0.16 | 0.31 | 4.33 | 2.37 |
| *Hylobates klossii* | 4 | X | 30.54 | 9.52 | 7.77 | 6.08 | 6.38 | 4.34 | 5.21 | 4.02 | 6.19 | 6.44 | 7.79 | 7.14 | 5.93 | 39.88 | – |
| | | SD | 1.53 | 0.26 | 0.23 | 0.15 | 0.17 | 0.14 | 0.14 | 0.33 | 0.56 | 0.18 | 0.16 | 0.10 | 0.17 | 1.62 | – |
| *Hylobates lar* | 8 | X | 36.35 | 11.30 | 8.27 | 6.07 | 6.02 | 4.69 | 5.07 | 4.40 | 5.86 | 6.92 | 8.72 | 7.55 | 6.27 | 47.32 | – |
| | | SD | 1.44 | 0.88 | 0.70 | 0.69 | 0.61 | 0.50 | 0.41 | 0.47 | 0.83 | 0.64 | 0.84 | 0.61 | 0.63 | 6.85 | – |
| *Hylobates muelleri* | 1 | X | 31.29 | 10.25 | 9.12 | 6.72 | 6.81 | 4.86 | 5.32 | 4.79 | 6.03 | 5.82 | 7.88 | 7.56 | 6.03 | 44.35 | – |
| *Lagothrix lagotricha* | 7 | X | 28.46 | 7.72 | 7.28 | 5.00 | 4.90 | 3.64 | 3.80 | 3.81 | 4.03 | 6.23 | 6.61 | 5.96 | 5.01 | 30.05 | 96.81 |
| | | SD | 1.96 | 0.44 | 0.76 | 0.45 | 0.35 | 0.36 | 0.28 | 0.33 | 0.42 | 0.63 | 0.58 | 0.43 | 0.42 | 5.52 | – |
| *Lophocebus albigena* | 6 | X | 35.70 | 8.67 | 9.14 | 5.51 | 6.16 | 4.30 | 4.89 | 4.10 | 4.86 | 7.36 | 6.91 | 7.01 | 5.63 | 50.39 | – |
| | | SD | 2.13 | 0.77 | 0.78 | 0.36 | 0.56 | 0.30 | 0.45 | 0.28 | 0.34 | 0.84 | 0.55 | 0.43 | 0.31 | 7.43 | – |
| *Macaca arctoides* | 1 | X | 25.86 | 8.27 | 7.43 | 5.40 | 6.23 | 3.70 | 4.43 | 3.50 | 4.67 | 5.92 | 7.17 | 6.29 | 5.13 | 37.11 | 98.89 |
| *Macaca fascicularis* | 11 | X | 26.29 | 6.99 | 6.47 | 4.10 | 4.93 | 3.16 | 3.68 | 2.79 | 3.82 | 4.82 | 5.77 | 5.24 | 4.14 | 24.39 | 98.25 |
| | | SD | 3.00 | 0.65 | 0.63 | 0.39 | 0.64 | 0.40 | 0.44 | 0.31 | 0.46 | 0.62 | 0.48 | 0.50 | 0.40 | 4.20 | 2.23 |
| *Macaca fuscata* | 2 | X | 30.14 | 9.74 | 8.24 | 5.87 | 6.90 | 3.93 | 5.09 | 3.83 | 4.92 | 6.86 | 7.91 | 7.00 | 5.65 | 45.11 | 98.99 |
| | | SD | 1.78 | 1.47 | 0.04 | 0.15 | 0.26 | 0.21 | 0.64 | 0.34 | 0.71 | 1.02 | 0.71 | 0.59 | 0.66 | 7.24 | – |
| *Macaca mulatta* | 16 | X | 31.89 | 9.76 | 8.44 | 5.84 | 6.70 | 4.27 | 5.17 | 4.10 | 5.38 | 6.92 | 7.90 | 7.20 | 5.89 | 46.34 | – |
| | | SD | 2.73 | 0.78 | 0.80 | 0.55 | 0.56 | 0.40 | 0.45 | 0.39 | 0.57 | 0.59 | 0.68 | 0.58 | 0.50 | 6.84 | – |
| *Macaca nemestrina* | 8 | X | 35.49 | 9.92 | 8.95 | 5.86 | 7.32 | 4.31 | 5.38 | 3.96 | 5.15 | 6.60 | 7.97 | 7.34 | 5.71 | 50.78 | 101.74 |
| | | SD | 4.65 | 1.52 | 1.40 | 0.86 | 1.41 | 0.49 | 1.07 | 0.56 | 1.09 | 1.10 | 1.17 | 1.13 | 0.91 | 14.45 | 3.33 |
| *Macaca tonkeana* | 5 | X | 34.56 | 10.03 | 9.28 | 6.23 | 7.38 | 4.58 | 5.31 | 4.22 | 5.14 | 6.87 | 8.22 | 7.52 | 5.91 | 51.71 | – |
| | | SD | 2.42 | 0.77 | 0.93 | 0.39 | 0.37 | 0.37 | 0.25 | 0.47 | 0.50 | 0.64 | 0.55 | 0.49 | 0.47 | 6.15 | – |
| *Mandrillus leucophaeus* | 1 | X | 41.30 | 14.09 | 11.74 | 9.77 | 9.34 | 6.58 | 6.83 | 5.64 | 7.18 | 8.28 | 10.56 | 9.99 | 7.71 | 85.63 | 99.91 |
| *Miopithecus ogouensis* | 1 | X | 15.66 | 4.20 | 4.48 | 2.70 | 3.21 | 1.95 | 2.44 | 1.98 | 2.62 | 2.97 | 3.93 | 3.41 | 2.79 | 10.66 | – |
| *Nasalis larvatus* | 16 | X | 41.49 | 11.93 | 11.04 | 7.30 | 7.98 | 5.41 | 6.39 | 5.49 | 6.74 | 8.82 | 9.97 | 9.10 | 7.55 | 62.92 | 93.30 |
| | | SD | 4.18 | 1.50 | 1.24 | 1.00 | 0.98 | 0.72 | 0.82 | 0.77 | 0.72 | 1.03 | 1.15 | 1.05 | 0.87 | 15.18 | 3.56 |
| *Nomascus concolor* | 2 | X | 38.29 | 10.53 | 9.06 | 5.74 | 5.78 | 4.36 | 4.92 | 4.63 | 5.62 | 6.86 | 8.30 | 7.43 | 6.20 | 51.49 | – |
| | | SD | 2.50 | 0.42 | 0.54 | 0.71 | 0.04 | 0.33 | 0.25 | 0.32 | 0.18 | 0.13 | 0.59 | 0.25 | 0.30 | 3.99 | – |
| *Pan paniscus* | 14 | X | 46.29 | 19.40 | 17.01 | 12.86 | 12.41 | 9.40 | 10.34 | 10.17 | 12.67 | 11.79 | 15.05 | 14.36 | 12.29 | 154.88 | 97.16 |
| | | SD | 2.44 | 1.41 | 1.59 | 1.02 | 1.34 | 0.65 | 0.87 | 0.72 | 1.19 | 0.69 | 1.20 | 0.94 | 0.77 | 22.89 | – |
| *Pan troglodytes schweinfurthii* | 1 | X | 59.23 | 23.82 | 18.73 | 16.64 | 12.24 | 10.83 | 10.91 | 10.57 | 13.58 | 14.35 | 14.88 | 16.15 | 13.23 | 238.92 | 95.76 |
| *Pan troglodytes troglodytes* | 12 | X | 52.59 | 20.24 | 17.23 | 13.80 | 11.22 | 9.56 | 10.43 | 10.34 | 13.30 | 13.55 | 15.18 | 14.85 | 12.93 | 176.15 | – |
| | | SD | 4.52 | 2.78 | 1.84 | 2.22 | 1.78 | 1.11 | 1.50 | 1.29 | 1.58 | 1.01 | 2.24 | 1.46 | 1.15 | 27.32 | – |
| *Pan troglodytes verus* | 3 | X | 52.52 | 21.43 | 16.59 | 14.02 | 10.79 | 9.95 | 10.13 | 11.23 | 13.69 | 13.29 | 16.00 | 15.09 | 13.44 | 192.27 | – |
| | | SD | 4.19 | 1.35 | 0.79 | 1.01 | 0.69 | 0.36 | 0.76 | 0.42 | 0.96 | 0.08 | 0.29 | 0.55 | 0.31 | 30.18 | – |
| *Papio anubis* | 2 | X | 40.54 | 13.30 | 10.41 | 8.60 | 8.92 | 6.01 | 6.63 | 5.24 | 6.72 | 9.24 | 10.60 | 9.53 | 7.65 | 79.74 | 97.25 |
| | | SD | 8.97 | 2.81 | 2.36 | 1.71 | 1.66 | 1.05 | 1.32 | 0.73 | 0.83 | 1.99 | 2.67 | 1.86 | 1.40 | 30.71 | – |
| *Papio cyncocephalus* | 2 | X | 35.81 | 11.21 | 9.99 | 7.26 | 7.22 | 4.89 | 5.42 | 4.77 | 5.69 | 7.93 | 9.10 | 8.17 | 6.65 | 62.27 | – |
| | | SD | 5.06 | 0.70 | 0.93 | 0.91 | 0.57 | 0.48 | 0.64 | 0.33 | 0.57 | 0.03 | 0.64 | 0.71 | 0.40 | 10.13 | – |
| *Papio hamadryas* | 1 | X | 32.87 | 10.57 | 8.65 | 6.62 | 7.19 | 4.59 | 5.32 | 4.39 | 5.46 | 7.89 | 8.82 | 7.72 | 6.39 | 55.39 | – |
| *Papio ursinus* | 10 | X | 37.12 | 11.39 | 10.19 | 7.50 | 7.75 | 5.27 | 5.99 | 5.02 | 6.28 | 7.87 | 9.61 | 8.58 | 6.98 | 62.81 | 97.54 |
| | | SD | 2.94 | 0.67 | 1.26 | 0.82 | 0.74 | 0.47 | 0.55 | 0.59 | 0.37 | 0.54 | 0.91 | 0.65 | 0.47 | 9.67 | 4.72 |
| *Piliocolobus badius* | 9 | X | 31.79 | 8.85 | 7.08 | 5.19 | 5.01 | 3.91 | 3.94 | 3.64 | 4.14 | 6.58 | 6.43 | 6.18 | 5.02 | 32.33 | 93.68 |
| | | SD | 2.37 | 0.37 | 0.48 | 0.43 | 0.46 | 0.26 | 0.25 | 0.15 | 0.25 | 0.43 | 0.59 | 0.34 | 0.27 | 3.42 | 1.49 |
| *Pithecia monachus* | 1 | X | 23.95 | 6.15 | 4.85 | 3.52 | 3.51 | 2.66 | 3.13 | 2.77 | 3.14 | 4.24 | 4.81 | 4.43 | 3.65 | 16.58 | – |
| *Pithecia pithecia* | 3 | X | 26.52 | 5.74 | 5.70 | 3.32 | 3.40 | 2.67 | 2.88 | 2.65 | 2.71 | 4.27 | 4.82 | 4.36 | 3.48 | 19.36 | 100.19 |
| | | SD | 0.78 | 0.48 | 0.49 | 0.46 | 0.29 | 0.27 | 0.32 | 0.37 | 0.27 | 0.24 | 0.17 | 0.21 | 0.11 | 0.92 | – |
| *Pongo abelii* | 11 | X | 40.27 | 15.77 | 13.64 | 11.28 | 11.17 | 8.19 | 9.23 | 8.03 | 10.95 | 9.13 | 12.79 | 12.07 | 10.04 | 94.76 | – |
| | | SD | 3.82 | 1.17 | 1.52 | 1.48 | 1.56 | 2.35 | 1.76 | 1.16 | 2.04 | 0.94 | 1.30 | 1.06 | 1.14 | 24.31 | – |
| *Pongo pygmaeus* | 19 | X | 44.52 | 17.59 | 15.02 | 12.42 | 11.65 | 8.13 | 8.83 | 8.13 | 11.18 | 10.00 | 13.36 | 12.73 | 10.48 | 132.42 | 89.23 |
| | | SD | 5.28 | 2.29 | 2.74 | 2.83 | 2.54 | 1.17 | 1.79 | 1.04 | 1.81 | 1.52 | 1.94 | 1.83 | 1.39 | 31.74 | 3.00 |
| *Presbytis comata* | 1 | X | 32.70 | 9.14 | 8.47 | 5.34 | 5.43 | 3.92 | 4.32 | 3.88 | 4.35 | 5.78 | 7.06 | 6.49 | 5.12 | 39.44 | – |
| *Presbytis frontata* | 1 | X | 32.08 | 8.19 | 8.48 | 4.95 | 5.10 | 4.83 | 4.50 | 3.89 | 4.23 | 5.16 | 7.27 | 6.41 | 4.98 | 32.17 | – |
| *Presbytis melalophos* | 2 | X | 33.11 | 8.85 | 7.74 | 5.02 | 4.94 | 4.03 | 4.38 | 3.79 | 4.48 | 5.55 | 6.79 | 6.31 | 5.02 | 35.45 | 100.05 |

| | | | | | | | | | | | | | | | | | | |
|---|---|---|---|---|---|---|---|---|---|---|---|---|---|---|---|---|---|---|
| | | SD | 1.06 | 0.68 | 0.35 | 0.07 | 0.04 | 0.01 | 0.07 | 0.01 | 0.01 | 0.59 | 0.46 | 0.03 | 0.05 | 0.81 | – | |
| *Presbytis rubicunda* | 4 | X | 31.37 | 8.49 | 7.16 | 4.75 | 5.10 | 3.67 | 4.19 | 3.27 | 4.30 | 5.75 | 6.65 | 6.02 | 4.81 | 30.96 | – | |
| | | SD | 2.50 | 0.57 | 0.45 | 0.25 | 0.25 | 0.57 | 0.11 | 0.29 | 0.33 | 0.44 | 0.41 | 0.33 | 0.32 | 3.14 | – | |
| *Procolobus verus* | 1 | X | 25.97 | 7.21 | 5.81 | 4.07 | 4.25 | 3.21 | 3.38 | 2.82 | 3.22 | 4.77 | 5.01 | 4.96 | 3.84 | 23.94 | – | |
| *Pygathrix nemaeus* | 3 | X | 37.68 | 10.39 | 9.69 | 6.41 | 6.68 | 4.60 | 5.26 | 4.66 | 5.97 | 8.42 | 8.80 | 7.94 | 6.72 | 57.31 | 97.37 | |
| | | SD | 4.55 | 1.24 | 0.26 | 0.15 | 0.44 | 0.17 | 0.21 | 0.09 | 0.24 | 1.32 | 0.82 | 0.31 | 0.32 | 13.03 | – | |
| *Rhinopithecus roxellana* | 2 | X | 33.43 | 9.70 | 8.82 | 6.37 | 5.96 | 4.46 | 4.58 | 4.15 | 5.15 | 7.59 | 7.09 | 7.16 | 5.82 | 49.83 | 90.64 | |
| | | SD | 1.17 | 0.30 | 1.03 | 0.52 | 0.42 | 0.37 | 0.32 | 0.30 | 0.17 | 1.20 | 0.06 | 0.45 | 0.39 | 1.46 | – | |
| *Saimiri boliviensis* | 8 | X | 15.81 | 4.31 | 3.43 | 2.31 | 2.61 | 1.66 | 2.10 | 1.86 | 2.09 | 3.11 | 3.14 | 3.01 | 2.48 | 7.67 | 100.01 | |
| | | SD | 1.08 | 0.18 | 0.18 | 0.15 | 0.21 | 0.12 | 0.24 | 0.13 | 0.10 | 0.20 | 0.27 | 0.17 | 0.14 | 1.04 | 3.17 | |
| *Sapajus apella* | 15 | X | 23.83 | 7.14 | 6.49 | 4.22 | 4.71 | 3.32 | 3.79 | 3.28 | 3.92 | 5.17 | 6.11 | 5.39 | 4.49 | 26.19 | 98.57 | |
| | | SD | 1.41 | 0.47 | 0.39 | 0.26 | 0.37 | 0.29 | 0.29 | 0.28 | 0.34 | 0.37 | 0.32 | 0.30 | 0.30 | 2.65 | 2.31 | |
| *Semnopithecus johnii* | 1 | X | 35.83 | 9.91 | 9.51 | 6.18 | 6.26 | 4.43 | 4.90 | 4.25 | 4.92 | 7.90 | 7.08 | 7.34 | 5.85 | 50.22 | – | |
| *Symphalangus syndactylus* | 5 | X | 40.30 | 11.82 | 10.42 | 6.77 | 6.74 | 4.93 | 5.83 | 4.80 | 6.68 | 9.70 | 8.61 | 8.52 | 7.19 | 66.75 | – | |
| | | SD | 2.36 | 0.84 | 1.49 | 0.70 | 0.51 | 0.47 | 0.32 | 0.40 | 0.39 | 0.66 | 0.83 | 0.58 | 0.50 | 5.42 | – | |
| *Theropithecus gelada* | 3 | X | 33.59 | 8.90 | 8.47 | 5.69 | 6.35 | 4.36 | 5.19 | 4.04 | 5.34 | 7.36 | 7.25 | 7.11 | 5.81 | 36.86 | 94.55 | |
| | | SD | 0.57 | 1.54 | 0.64 | 0.62 | 0.80 | 0.55 | 0.73 | 0.37 | 0.69 | 0.67 | 0.33 | 0.59 | 0.25 | 4.47 | – | |
| *Trachypithecus auratus* | 2 | X | 32.35 | 8.30 | 7.79 | 5.96 | 5.81 | 4.18 | 4.48 | 3.57 | 4.51 | 6.21 | 6.02 | 6.45 | 4.94 | 36.01 | – | |
| | | SD | 0.04 | 0.04 | 0.13 | 0.01 | 0.07 | 0.01 | 0.03 | 0.01 | 0.04 | 0.42 | 0.71 | 0.03 | 0.05 | 1.53 | – | |
| *Trachypithecus cristatus* | 12 | X | 31.24 | 7.76 | 7.48 | 4.78 | 5.27 | 3.71 | 4.37 | 3.47 | 4.12 | 6.07 | 6.22 | 6.05 | 4.82 | 25.92 | – | |
| | | SD | 1.64 | 0.49 | 0.49 | 0.29 | 0.30 | 0.23 | 0.48 | 0.23 | 0.30 | 0.48 | 0.45 | 0.36 | 0.31 | 3.54 | 95.57 | |
| *Trachypithecus obscurus* | 2 | X | 30.23 | 8.45 | 8.49 | 5.39 | 6.16 | 3.95 | 4.91 | 3.82 | 4.47 | 6.10 | 6.50 | 6.54 | 5.10 | 36.81 | – | |
| | | SD | 0.06 | 0.18 | 0.60 | 0.04 | 0.01 | 0.01 | 0.01 | 0.01 | 0.02 | 0.57 | 0.22 | 0.11 | 0.17 | 1.35 | – | |

[a] X, mean; SD, one standard deviation; IAL, interarticular length; DPH, dorsoplantar height, MLW, mediolateral width; B, base; H, head; 25%, 25% of shaft length from the proximal end; 50%, midshaft; 75%, 75% of shaft length from the proximal end; GMean, geometric mean; (11), eleven variables; (Di), distal four variables; CunM Area, area of the proximal articular surface; PAA, physiological abduction angle. See text and Figure 2 for measurement details.

[b] No SD is reported for species with only 1 specimen.

[c] Data from Goodenberger et al., 2015.

(Fig. 2): base (B); 25% of shaft length from the proximal end (25%); midshaft or 50% of shaft length (50%); 75% of shaft length from the proximal end (75%); and head (H). The location for the H-DPH and H-MLW measurements were identified where the head is the widest in dorsal view. The DPH and MLW linear measurements were standardized at all locations by obtaining transverse two-dimensional (2D) cross-sections using the Intersect function and then using the BoundingBox function to determine maximum dimensions in dorsoplantar and mediolateral orientations (Fig. 2D). The maximum heights and widths of the bounding box for the transverse cross-sections approximates the same measurements that would be taken with standard calipers, but with greater replicability (and with a digital record of the results to facilitate review if needed). The area (in $mm^2$) of the proximal articular facet for the medial cuneiform (CunM Area) was quantified for each specimen using Geomagic Studio software (Fig. 2E). Segmentation of the proximal articular surface was accomplished by selecting the relevant polygon mesh triangles with the aid of a stylus and a Wacom Cintiq interactive display. A physiological abduction angle with Mt1s in dorsolateral view (PAA, sensu Boyer et al., 2007; Jacobs et al., 2009) was measured on the complete fossils (and estimated for fragmentary ones) and these data were compared to previously published values for extant and fossil anthropoid samples (Patel et al., 2012; Goodenberger et al., 2015).

Six indices were created as ratios of the linear and area measurements: (1) relative length index: IAL divided by the square root of the CunM Area; (2) midshaft robusticity index: the average of 50%-DPH and 50%-MLW divided by IAL; (3) proximodistal shaft tapering index: 75%-MLW divided by 25%-MLW; (4) distal shaft to head expansion index: 75%-MLW divided by H-MLW; (5) head shape index: H-DPH divided by H-MLW; (6) base shape index: B-DPH divided by B-MLW. Collectively, all these data were used to make informative assessments on the comparative and functional morphology of the fossil Mt1s.

### 2.3. Multivariate analysis of Mt1 shape

To further assess overall Mt1 shape, a multivariate principal components analysis (PCA) was performed with the entire extant sample, the most complete Songhor Mt1 specimen (KNM-SO 31233), and other complete fossil Mt1s. The variables included were the 11 linear dimensions described above, which were size-adjusted by dividing each by the square root of CunM Area (see Supplementary Online Material [SOM] Table S1 for raw data). CunM Area was implemented as the size proxy instead of the geometric mean (GMean) of the same linear dimensions as is often done (e.g., Jungers et al., 1995) because this variable is independent from the linear measurements. As is also discussed below, CunM Area was found to be a robust variable to make predictions of body mass. The PCA was performed in PAST v.3.11 software (Hammer et al., 2001).

### 2.4. Taxonomic assessment from molar size predictions

To better attribute the Songhor fossil Mt1s to specific taxa currently known at Songhor, second lower molar ($M_2$) mesiodistal length (MDL) was predicted from several Mt1 size proxy variables (Table 1). The first Mt1 variable was a whole-bone geometric mean (Jungers et al., 1995) calculated from all 11 linear variables and is referred to as GMean(11). The GMean(11) variable was applicable for only KNM-SO 31233 since it is the only complete Songhor Mt1. Because KNM-SO 22235 is only a distal fragment, a second variant of the geometric mean was calculated from the four distal-most linear variables [75%-DPH, 75%-MLW, H-DPH and H-MLW] and is referred to as GMean(Di). Unfortunately, all four of these distal variables were not preserved in KNM-SO 5129 so it was excluded

**Table 2**
Fossil sample and data for Mt1 variables.[a]

| Fossil Specimen – Taxon[g] | IAL | B-DPH | B-MLW | 25%-DPH | 25%-MLW | 50%-DPH | 50%-MLW | 75%-DPH | 75%-MLW | H-DPH | H-MLW | GMean(11) | GMean(Di) | CunM Area | PAA | Data Ref.[e] |
|---|---|---|---|---|---|---|---|---|---|---|---|---|---|---|---|---|
| KNM-SO 31233 | 36.31 | 8.21 | 8.99 | 4.87 | 5.87 | 4.16 | 4.89 | 4.22 | 5.02 | 6.49 | 7.5[b] | 6.87 | 5.67 | 43.75 | 101.0 | 1 |
| KNM-SO 1080 | – | 11.00 | 9.10 | 5.90 | 6.30 | 4.50 | 5.40 | 4.30 | 4.60 | – | – | – | – | 53.64 | 96.0[f] | 1 |
| KNM-SO 5129 | – | – | – | – | – | – | – | 5.00 | 5.80 | 7.80 | – | – | – | – | – | 1 |
| KNM-SO 5141 | – | 22.60 | 19.20 | – | – | – | – | – | – | – | – | – | – | 189.43 | 114.0[f] | 1 |
| KNM-SO 22235 | – | – | – | – | – | – | – | 5.80 | 6.50 | 9.50[c] | 10.40[c] | – | 7.81 | – | – | 1 |
| DPC 13318 – *Aegyptopithecus zeuxis* | 27.70 | 9.72 | 6.87 | 6.49 | 6.56 | 4.44 | 4.83 | 4.30 | 5.10 | 5.85 | 6.22 | 6.76 | 5.31 | 37.11 | 96.8[d] | 1 |
| YPM 25806 – *Aegyptopithecus zeuxis* | – | 10.08 | 9.42 | – | – | – | – | – | – | – | – | – | – | 43.98 | 99.5[f] | 1 |
| DPC 20939 – *Catopithecus browni* | 14.38 | 3.81 | 3.13 | 2.39 | 2.63 | 1.91 | 1.92 | 1.72 | 2.06 | 2.64 | 3.60 | 2.92 | 2.41 | 5.75 | 100.5[d] | 1 |
| *Epipliopithecus vindobonensis* (Individual 1) | 37.65 | 10.59 | 9.85 | 7.48 | 6.85 | 5.58 | 5.45 | 5.77 | 6.04 | 8.45 | 8.71 | 8.45 | 7.12 | 59.17 | 98.3 | 1 |
| *Epipliopithecus vindobonensis* (Individual 2) | 38.80 | 11.10 | 10.18 | 7.71 | 6.89 | 5.29 | 5.40 | 5.43 | 5.96 | 9.01 | 8.90 | 8.52 | 7.14 | 61.99 | 99.6 | 1 |
| *Epipliopithecus vindobonensis* (Individual 3) | 38.88 | 11.33 | 10.14 | 7.84 | 6.88 | 5.53 | 5.32 | 5.67 | 6.02 | 8.96 | 8.96 | 8.62 | 7.24 | 60.86 | 101.0 | 1 |
| KNM-CA 1865 – *Proconsul* cf. *africanus* | – | 11.30 | 10.10 | – | – | – | – | – | – | – | – | – | – | – | – | 2 |
| KNM-CA 1889 – *Proconsul* cf. *africanus* | – | – | – | – | – | – | – | – | | 9.20 | 9.80 | – | – | – | – | 2 |
| KNM CA 2236 – *Proconsul* cf. *africanus* | – | – | – | – | – | – | – | – | – | 7.60 | 8.50 | – | – | – | – | 2 |
| KNM-CA 2239 – *Proconsul* cf. *africanus* | – | – | – | – | – | – | – | – | – | 8.50 | 9.80 | – | – | – | – | 2 |
| KNM-KPS III – *Ekembo heseloni* | 38.00 | 12.21 | – | 7.94 | 6.40 | 5.64 | 6.17 | 5.43 | 6.33 | 9.03 | 9.66 | – | 7.40 | – | 101.0[f] | 1 |
| KNM-KPS VIII – *Ekembo heseloni* | 39.00 | – | – | – | – | – | – | – | – | 8.40 | 10.20 | – | – | – | – | 1 |
| KNM-RU 15074 – *Ekembo heseloni* | – | – | – | – | – | – | – | – | – | – | – | – | – | – | – | 4 |
| KNM-RU 17392 – *Ekembo nyanzae* | 53.80 | 16.80 | 13.89 | 12.56 | 11.12 | 8.86 | 8.98 | 8.25 | 9.18 | 11.90 | 12.92 | 12.88 | 10.39 | 127.89 | 103.0 | 1 |
| KNM-RU 2036 – *Ekembo heseloni* | 34.03 | 10.35 | 10.16 | 8.06 | 8.02 | 5.52 | 5.93 | 5.24 | 6.64 | 6.77 | 7.83 | 8.36 | 6.55 | 70.33 | 97.0 | 1 |
| KNM-RU 5872 – *Ekembo nyanzae* | 51.12 | 16.98 | 14.79 | 12.12 | 11.46 | 8.28 | 8.93 | 7.33 | 9.81 | 11.90 | 14.29 | 12.88 | 10.52 | 128.17 | 102.0 | 1 |
| KNM-WK 18119 – *Afropithecus turkanensis* | – | 17.32 | 13.66 | – | – | – | – | – | – | – | – | – | – | 123.16 | 99.0[f] | 1 |
| KNM-BG 17814 – *Nacholapithecus kerioi* | – | – | – | – | – | – | – | – | – | – | – | – | – | – | – | 4 |
| GSP 14046 – *Sivapithecus parvada* | – | – | – | – | – | – | – | – | – | 14.80 | 16.30 | – | – | – | – | 3 |

[a] IAL, interarticular length; DPH, dorsoplantar height, MLW, mediolateral width; B, base; H, head; 25%, 25% of shaft length from the proximal end; 50%, midshaft; 75%, 75% of shaft length from the proximal end; GMean, geometric mean; (11), eleven variables; (Di), distal four variables; CunM Area, area of the proximal articular surface; PAA, physiological abduction angle. See text and Figure 2 for measurement details.
[b] Minimum estimated value used in all analyses; actual preserved length is 6.9 mm (see text).
[c] Preserved length.
[d] Data from Goodenberger et al., 2015.
[e] Original data source: (1) this study; (2) Harrison and Andrews, 2009; (3) Pilbeam et al., 1980; (4) Rose et al., 1996
[f] Estimated values.
[g] Fossils with no data are included here to make readers aware of the existence of these specimens and to indicate that no data were obtainable for this study.

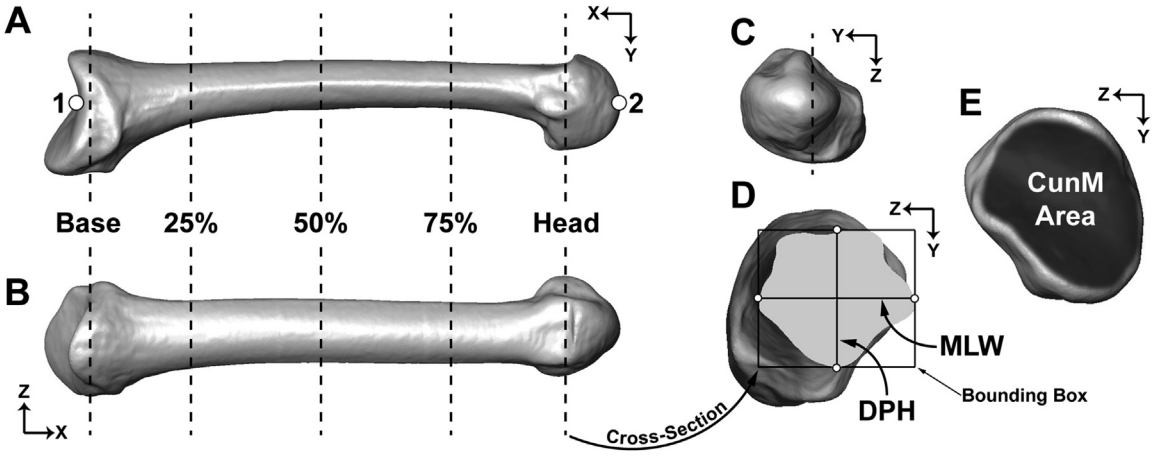


**Figure 2.** Virtual reconstruction of a *Pithecia pithecia* left Mt1 in standardized orientation shown in (A) medial, (B) dorsal, (C) distal, and (E) proximal views. The vertical dashed line in (C) represents the plane at the deepest level of the head's sesamoid gutters. See text for specific information about the orientation protocol. Interarticular Length [IAL] was measured between Landmarks 1 and 2 on the proximal and distal articular surfaces, respectively. Dorsoplantar Height [DPH] and Mediolateral Width [MLW] were measured at five locations – Base, 25% of shaft length, midshaft or 50% of shaft length, 75% of shaft length, Head – and are shown with the dashed vertical lines in (A) and (B). As illustrated in (D), a Cross-Section and Bounding Box was used to systematically identify DPH and MLW. The area of the proximal articular surface [CunM Area] was quantified by segmenting out the proximal articular surface as shown by the dark region in (E).

from this analysis. Because KNM-SO 1080 and KNM-SO 5141 have only well-preserved proximal ends, the third variable used to predict $M_2$ MDL was the square root of CunM Area. The natural log of $M_2$ MDL was regressed (using ordinary least-squares methods, OLS) against the natural log of GMean(11), GMean(Di), and the square-root of CunM Area. These analyses used sex-specific means for the extant sample and corresponding sex-specific $M_2$ MDL were obtained from the literature (Swindler, 2002) or from specimens directly measured by the authors. The resulting dataset included 79 sex-specific mean values (see SOM Table S2). Using the calculated regression lines (SOM Table S3), we predicted the natural log of $M_2$ MDL (and the 95% confidence interval [CI] and 95% prediction interval [PI]) expected for an individual with Mt1 size variables similar to our fossils. Regression analyses were conducted in SPSS 16.0 software and fossil 95% CIs and PIs were calculated by hand using Equation 17.29 in Zar (1984). The resulting predictions were compared to the natural log of $M_2$ MDL of Songhor specimens with known taxonomic attributions (Andrews, 1978; Hill et al., 2013; see SOM Table S4 for Songhor tooth metrics).

### 2.5. Taxonomic assessment from body mass predictions

To predict the body masses of the primates in the Songhor Mt1 assemblage, as well as for other fossil catarrhines with well-preserved Mt1s, three body mass prediction equations were generated from the extant comparative sample ($n = 404$). The independent variables for Mt1 size included: 1) the square root of CunM Area; 2) GMean(11); and 3) the square root of the product of H-DPH and H-MLW (see Table 1). The latter measure based on two head dimensions was used in this analysis (instead of the GMean(Di) size variable used in the $M_2$ predictions discussed above) so that more Miocene fossil taxa/specimens could be included. KNM-SO 5129 was excluded from this analysis because a H-MLW was not obtainable. Male and female body masses were compiled from Smith and Jungers (1997), Smith et al. (2003), and Isler et al. (2008). Specimens were averaged into sex-specific means if dimorphism exceeded 20% (dimorphism % = ln[male body mass]-ln[female body mass]*100), following Yapuncich et al. (2015). If dimorphism was less than 20%, male and female specimens were averaged into species means. The resulting dataset included 111 species or sex-specific mean values (see SOM Table S5). All three predictor variables were natural-log transformed and regressed against the natural-log transformed cube root of body mass using OLS regression. Precision and accuracy of these equations were evaluated with the coefficient of determination ($r^2$), mean square error (MSE), percent standard error of the estimate (%SEE), and predicted residual sum of squares (PRESS). As the reference samples were comprised of species or sex-specific means, fossil body masses were predicted from mean values of the predictor variables whenever possible to avoid changing the units of analysis (Yapuncich, 2017). Quasi-maximum likelihood estimators (QMLE = exp[MSE/2]) were applied to correct for bias when de-transforming logged data (Sprugel, 1983; Smith, 1993) and all fossil body masses are bracketed by 95% PIs.

## 3. Results

### 3.1. Fossil descriptions

3.1.1. KNM-SO 31233 KNM-SO 31233 is a complete left Mt1 from a small-to-medium-sized anthropoid primate (Fig. 1; Table 2). Its maximum length is 38.8 mm and its proximodistal interarticular length is 36.3 mm. The shaft of the specimen was broken post-fossilization ~18.0 mm from its distal articular surface. Despite being in two pieces, the shaft is not distorted in any appreciable way and has a midshaft dorsoplantar and a mediolateral diameter of 4.2 mm and 4.9 mm, respectively; as such it is gracile (i.e., relatively narrow for its length). The cross-sectional shape of the diaphysis gradually tapers from proximal to distal; it is dorsoplantarly taller and mediolaterally wider proximally and dorsoplantarly shorter and mediolaterally narrower distally. The dorsoplantar height and mediolateral widths at the 25% position of shaft length are 4.9 mm and 5.9 mm, respectively, and are 4.2 mm and 5.0 mm, respectively, at the 75% position. There is a presence of a weak rugosity on the dorsomedial side of the shaft just proximal to the head that likely is an attachment site of the metatarsophalangeal (MTP) joint capsule, or may contribute to the insertion of the abductor hallucis muscle. The specimen's head has a dorsoplantar height of 6.5 mm and a preserved mediolateral width of 6.9 mm. The lateral distal epicondyle is partially broken, but if fully preserved the head's mediolateral width would likely have been between 7.5 and 8.0 mm; the

minimum estimated measure of 7.5 mm is used for H-MLW in all analyses. (Note that a reconstructed lateral epicondyle is illustrated in Figure 4). The medial side of the head has some abrasion but the medial epicondyle appears to be intact. Its proximal base has a dorsoplantar height of 8.2 mm and a mediolateral width of 9.0 mm. There is substantial diaphyseal torsion, i.e., the long axis of the proximal articular surface is oriented almost 45° laterally when viewed from the proximal end. The proximal articular surface for the medial cuneiform has an area of 43.8 $mm^2$, and its shape resembles an elongated ellipse with minimal lateral notching. The medioplantar side of the base has a facet for a prehallux (a small sesamoid or sesamoid-like bone [i.e., typically ossified] within the tendon of the tibialis anterior muscle near the Mt1-medial cuneiform articulation), and the base's plantar side has a distinct insertion site for the peroneus longus muscle. The relatively small and short peroneal process is also dorsoplantarly shallow and is flat on its plantar surface. The proximal articular surface is a modified ovoid and is not sellar- or saddle-shaped. That is to say it is deeply concave from medial to lateral, but relatively flat from dorsal to plantar. In dorsolateral view with respect to the distal end of the bone, the proximal articular surface is only slightly concave. In the same view, this specimen has a PAA of 101°, indicating a moderate amount of abduction in the neutral position. The proximal articular surface does not extend dorsally and distally. In the same view, there is only a shallow notch located just proximal to the distal articular surface on the dorsal side of the bone. In dorsal view with respect to the distal end of the bone, the head's midline keel extends distally beyond the plane of the distal epicondyles. The extent of asymmetry in the distal epicondyles is unclear (since the lateral one is abraded), but the head lacks a distinct medial sesamoid gutter (facet) on the plantar side of the medial epicondyle. In distal view and with the preserved morphology, it appears that the medial sesamoid facet is oriented more obliquely (compared to the lateral facet) relative to the horizontal. Also, the head has a slight dorsal projection on its lateral side when viewed distally.

3.1.2. KNM-SO 1080 KNM-SO 1080 is a partial left Mt1 from a medium-to-small-sized anthropoid primate (Fig. 1; Table 2). The National Museums of Kenya fossil catalogue indicates that there are two pieces, a distal head and a fragment consisting of the proximal two-thirds of the bone. On closer inspection, these two pieces cannot come from the same bone because 1) the distal piece is too small to fit with the proximal fragment, and 2) the distal piece's morphology indicates that it comes from a non-pollical metacarpal. The latter has also been noted by Harrison (1982) and therefore the distal piece is not discussed further. KNM-SO 1080 represents approximately 65–75% of the entire Mt1 from the proximal end; ~26.3 mm measured from the proximal most end of the peroneal process. It too is composed of two pieces that have been fitted back together approximately 10.0 mm from the proximal end. It has a proximal base with a dorsoplantar height of 11.0 mm and a mediolateral width of 9.1 mm. The region that approximates midshaft has a dorsoplantar height of 4.5 mm and a mediolateral width of 5.4 mm. Near the 25% position along the shaft, the dimensions are 5.9 mm and 6.3 mm in dorsoplantar and mediolateral direction, respectively. The preserved distal end of the shaft, which approximates the 65–75% position, has a dorsoplantar diameter of 4.3 mm and a mediolateral diameter of 4.6 mm. These dimensions from the proximal end to the preserved distal end of the bone indicate that the shaft gradually tapers as it approaches the head. Without its head, however, it is not possible to describe its axial torsion. The proximal articular surface for the medial cuneiform is preserved and has an area of 53.6 $mm^2$; there is some minor damage to the lateral side of the base, but this does not impact area measurements. There is also some taphonomic damage to the dorsomedial side of the base. The overall shape of the proximal articular surface is concave-ovoid (and is not saddle-shaped) and has a distinct lateral notch that is easily seen in proximal view. This indicates a greater concavity from medial to lateral, but a relatively flat surface from dorsal to plantar. The medioplantar side of the base shows signs of having a prehallux facet, but the morphology is not clear due to some abrasion. The base's plantar side has a discrete insertion site for the peroneus longus muscle; the peroneal process is dorsoplantarly shallow and is flat on its plantar surface. In dorsolateral view with respect to the proximal end of the bone, the proximal articular surface is only slightly concave. In this same view, it would appear that the hallux would be slightly abducted when articulating with the medial cuneiform in the neutral position. Because the diaphysis is broken distally, a PAA is only estimated at 97°. Finally, there is a weak midline projection or keel that extends proximally beyond the plane of the proximal articular surface when viewed dorsally.

3.1.3. KNM-SO 5129 KNM-SO 5129 is a fragmentary right Mt1 from a medium-to-small-sized anthropoid primate (Fig. 1; Table 2). Only a ~12.0 mm segment (measured from the distal-most end of the head) is preserved. There is extensive abrasion on the medial side resulting in a broken medial epicondyle. The head measures 7.8 mm dorsoplantarly. The lateral distal epicondyle is intact and is robust, but it is unclear how asymmetrical the epicondyles may have been. The pit for the lateral collateral ligament is deep. In distal view, the medial sesamoid facet is oriented more obliquely relative to the horizontal compared to the preserved part of the lateral facet. Also in this view, the head is ovoid in shape, but it is unclear if the head is taller than it is wide. The preserved proximal end of the shaft, which likely approximates the 75% position, has a dorsoplantar diameter of 5.0 mm and a mediolateral diameter of 5.8 mm. Without more of the shaft and its proximal base, it is impossible to comment on its overall robusticity or degree of axial torsion.

3.1.4. KNM-SO 5141 KNM-SO 5141 is a partial left Mt1 from a large anthropoid primate (Fig. 1; Table 2). Only a ~25.1 mm segment (measured from the proximal most end of the peroneal process) is preserved. It has a proximal base with dorsoplantar height of 22.6 mm and mediolateral width of 19.2 mm. The preserved distal end of the shaft, which likely approximates the 25% position, has a dorsoplantar diameter of 11.6 mm and a mediolateral diameter of 12.7 mm. Without more of the shaft and its head, it is impossible to comment definitively on its degree of torsion and overall robusticity (which appears to be large). The proximal articular surface for the medial cuneiform, which has an area of 189.43 $mm^2$, is well-preserved except for two small quadrangular defects on its lateroplantar side. The overall shape of the proximal articular surface is concave-ovoid and is not saddle-shaped. It is not completely evident if the medioplantar side of the base has a facet for a prehallux. The base's plantar side has a distinct insertion site for the peroneus longus muscle; the peroneal process is dorsoplantarly shallow and is flat on its plantar surface. In dorsal view, it is clear that there is extensive asymmetry between the lateral and medial proximal-most aspect of the proximal articular surface. In dorsolateral view with respect to the proximal end of the bone, the proximal articular surface is significantly concave with a hint of a saddle shape. In this same view, it would appear that the hallux would have been substantially abducted when articulating with the medial cuneiform in the neutral position, but because most of the diaphysis is not present, a PAA is difficult to determine accurately.

However, with only the preserved portion, we cautiously estimate this value to be 114°.

3.1.5. KNM-SO 22235 KNM-SO 22235 is a partial right Mt1 from a medium-sized anthropoid primate (Fig. 1; Table 2). Only a ~18.2 mm segment (measured from the distal-most end of the head) is preserved. The head's distal articular surface has a small oval-shaped taphonomic defect on its dorsomedial side, and there is abrasion of its proximoplantar-most aspect. The head measures ~9.5 mm dorsoplantarly and ~10.4 mm mediolaterally. Without the abrasion, the head's dorsoplantar height could have been closer to 10.0–10.2 mm. The lateral distal epicondyle is intact (except for a small quadrangular shaped erosion) whereas some of the medial epicondyle has been broken. If it was intact and the entire plantar aspect of the head was present, it is likely that the epicondyles would be asymmetrical with the lateral side being larger. As a result, the lateral sesamoid gutter (facet) on the plantar side was likely slightly deeper; and by extension the lateral sesamoid bone for the lateral head of the flexor hallucis brevis muscle (and likely the adductor hallucis muscle) was possibly larger. In distal view, the medial sesamoid facet is oriented more obliquely relative to the horizontal compared to the lateral facet. Also in this view, the head is ovoid in shape and has a slight dorsal projection on its lateral side. The preserved proximal end of the shaft, which likely approximates the 75% position, has a dorsoplantar diameter of 5.8 mm and a mediolateral diameter of 6.5 mm. Without more of the shaft and its proximal base, it is impossible to comment on its overall robusticity and degree of axial torsion. There is a well-developed rugosity on the dorsomedial side of the shaft just proximal to the head, and the head has a dorsal projection on its lateral side when viewed distally.

### 3.2. Anatomical comparisons

Figures 3–5 provide medial, dorsal, proximal and distal views of representative extant and fossil Mt1s to facilitate anatomical comparisons with the Songhor specimens. Downloadable 3D models of these specimens are available at http://morphosource.org (see Appendix for details). Tables 1 and 3 along with Figure 6 help to further illustrate the comparisons.

The most striking feature of KNM-SO 31233 is its relatively long length. Relative to CunM (our body size proxy) its IAL is much more similar to hylobatids and both New and Old World monkeys, and different from great apes, which all have relatively short Mt1s (Fig. 6A). Moreover, KNM-SO 31233 falls within the upper range of most of these non-great ape taxa. It is important to highlight that this differs from measures of relative Mt1 length reported by others (e.g., Schultz, 1963; Langdon, 1986). Previously, researchers have characterized African apes and hylobatids as having long Mt1s relative to the lengths of their lateral metatarsals, whereas monkeys and *Pongo* have been described as having relatively short Mt1s. But without having any other metatarsals for comparison, an alternative scaling variable here is to use a proxy for overall size. The only fossil catarrhine that has a relatively longer Mt1 is *C. browni* (DPC 20939), whereas specimens attributed to *Aegyptopithecus* (DPC 13318) and *Ekembo* (KNM-RU 2036, 5872, 17392) are relatively shorter and overlap with the lower ranges of hylobatids and monkeys as well as the upper range of *Pan* and *Pongo*; the three specimens for *Epipliopithecus* have an intermediate relative length, but outside the great ape range (Fig. 6A, see Index 1 in Table 3).

KNM-SO 31233 also has a slender diaphysis relative to its length. Relative midshaft robusticity, measured as the average of 50%-DPH and 50%-MLW divided by IAL, is low in this fossil and is at the lower end of the hylobatid and monkey distributions (Fig. 6B). Again, extant great apes are different because they have the most robust Mt1 midshafts of all extant anthropoids except humans (Harrison, 1982; Conroy and Rose, 1983; Langdon, 1986). Though its shaft is not as slender as most pithecids, it does overlap with colobines and atelines. *Alouatta* has a much more robust shaft than KNM-SO 31233. The fragmentary nature of the other Songhor Mt1s prevents us from saying anything with confidence, but it is probable that KNM-SO 1080 had a relatively slender shaft, like monkeys and hylobatids, while KNM-SO 5141 may have been more robust, like extant great apes. The former is confirmed when evaluating midshaft robusticity relative to CunM Area (not shown here). KNM-SO 31233 is more gracile than all other fossil catarrhines sampled; all fossils studied here are more gracile than extant great apes (Fig. 6B, see Index 2 in Table 3). Among these, specimens belonging to *Aegyptopithecus* (DPC 13318) and *Ekembo* (KNM-RU 2036, 5872, 17392) have relatively robust midshafts that are within the upper range of hylobatids, cercopithecoids, *Alouatta* and *Sapajus*. Although KNM-KPS III specimen (*E. heseloni*) is not as robust as its other counterparts from Rusinga Island (which may be due to some mediolateral compression in the diaphysis), it is still relatively more robust than the complete Songhor Mt1 and those of *Epipliopithecus*.

All anthropoid Mt1s have some degree of proximodistal tapering of the diaphysis (Fig. 6C). In extant African apes, and to a lesser degree *Pongo* and hylobatids, the distal end of the diaphysis (at 75% of length) is wider than the proximal end (at 25% of length). KNM-SO 31233 is more similar to monkeys in having a proximodistal tapering shaft (especially in the mediolateral plane) with the wider side being proximal rather than distal. The same morphology can be seen in KNM-SO 1080 which overlaps the lower end of the cercopithecine and pithecid samples. Among the other fossils, only KNM-KPS III shows minimal shaft tapering like that seen in *Pongo* and hylobatids (Fig. 6C; see Index 3 in Table 3).

The relatively narrow breadth of the distal end of the diaphysis (at 75% of shaft length) in KNM-SO 31233, as well as KNM-SO 22235, is further evident when compared to its mediolaterally expanded head, which is also seen in most monkeys and to a lesser extent in *Alouatta* and hylobatids (Figs. 4 and 6D). Among the catarrhine fossil Mt1s, there is substantial variation both between- and within-species in relative head expansion (see Index 4 in Table 3). Specimens in the lower range of distal shaft compression relative to head width are *Catopithecus* (DPC 20939) and the one from Nachola (KNM-BG 17814; see also Rose et al., 1996) making them similar to monkeys. This is most likely related to them having well-developed medial and lateral epicondyles. At the other end of the spectrum, *Aegyptopithecus* (DPC 13318) and *E. heseloni* (KNM-RU 2036) show greater symmetry in H-MLW and 75%-MLW, similar to most specimens of *Pan* and *Pongo*. The specimen attributed to *Sivapithecus* (GSP 14046; Rose et al., 1996) is nearly identical to KNM-SO 22235 in this morphology.

Great apes, most hylobatids and most cercopithecines have heads that are dorsoplantarly short which make them appear to be wider than tall. Despite the large amount of overlap, colobine monkeys and platyrrhines (especially *Alouatta*), in general, have heads that are relatively taller than wide (see also Harrison, 1982). KNM-SO 31233 and 22235 are in between and within overlapping ranges of these two groups (Fig. 6E); this feature is not measurable in KNM-SO 5129. The *Epipliopithecus* Mt1s are distinctly different from the other fossil catarrhines in having heads that are only slightly wider than they are tall, although all three specimens are within the ranges for colobine monkeys and *Alouatta* (see Index 5 in Table 3).

Both KNM-SO 31233 and 22235 show signs of well-developed sesamoid gutters on the plantar side of the head, but there is asymmetry with the lateral side being more developed (or appearing to be since there is some abrasion as noted above). This

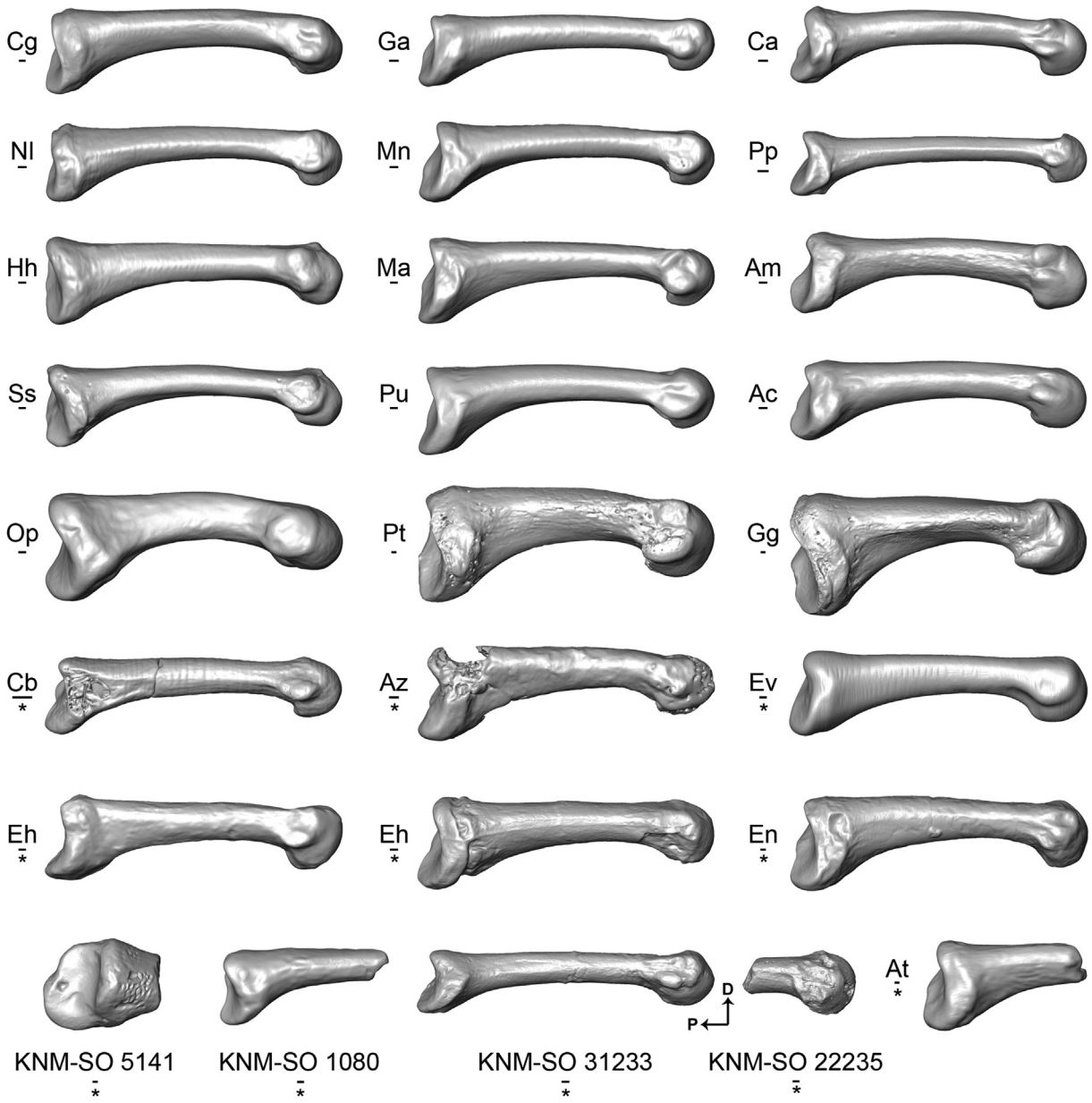


**Figure 3.** Representative virtual reconstructions of extant and fossil Mt1s in medial view (with respect to the bone's distal end). The fossils specimens are indicated by an asterisk (*). All specimens are originally from the left side except the following which have been mirror-imaged: KNM-RU 2036; KNM-KPS III; KNM-WK 18119; KNM-SO 22235. Dorsal is to the top and proximal is to the left. Taxonomic abbreviations: Ac, *Alouatta caraya*; Am, *Ateles marginatus*; At, *Afropithecus turkanensis* (KNM-WK 18119); Az; *Aegyptopithecus zeuxis* (DPC 13318); Ca, *Cebus albifrons*; Cb; *Catopithecus browni* (DPC 20939); Cg, *Colobus guereza*; Ev, *Epipliopithecus vindobonensis* (Ind. 3); Eh, *Ekembo heseloni* (KNM-KPS III is on the left and KNM-RU 2036 is in the center); En, *Ekembo nyanzae* (KNM-RU 5872); Ga, *Cercopithecus ascanius*; Gg, *Gorilla gorilla*; Hh, *Hoolock hoolock*; Ma; *Cercocebus galeritus*; Mn, *Macaca nemestrina*; Nl, *Nasalis larvatus*; Op, *Pongo pygmaeus*; Pp, *Pithecia pithecia*; Pt, *Pan troglodytes*; Pu, *Papio ursinus*; Ss, *Symphalangus syndactylus*. Scale bars below species/specimen number equal 1 mm. See Appendix for ID numbers of extant specimens.

asymmetrical morphology is similar to platyrrhines because of relatively larger lateral epicondyles (Fig. 5). In contrast, extant great apes also have a distinct asymmetry but the medial side is more developed (see Rose et al., 1996 for differing interpretation of ape Mt1 head morphology). Although hylobatids have a large lateral epicondyle, like platyrrhines, their medial epicondyle is more robust, like that of great apes. Only cercopithecoids appear to have more symmetrical lateral and medial epicondyle development. The symmetrical epicondyle development in cercopithecoids is not seen in any of the Songhor Mt1s or in most of the other fossil catarrhines (Fig. 5; see also Figure 45 in Pilbeam et al., 1980; see also Figure 22 in Rose et al., 1996). The *Catopithecus* Mt1 (DPC 20939), however, is the one fossil catarrhine that looks most like extant cercopithecoids, with more symmetrical bilateral epicondyle development.

The lateral dorsal projection just proximal to the distal articular surface seen in distal view on both KNM-SO 31233 and 22235 is common in other fossil catarrhines (Fig. 5). In general, all anthropoids studied here have this morphology (see also Harrison, 1982). Only extant hominoids also have a dorsal projection on the medial side just proximal to the distal articular surface. These projections contribute to attachment sites for the MTP joint capsule, suggesting that extant hominoids, in contrast to monkeys and fossil catarrhines, have more stable MTP1 joints.

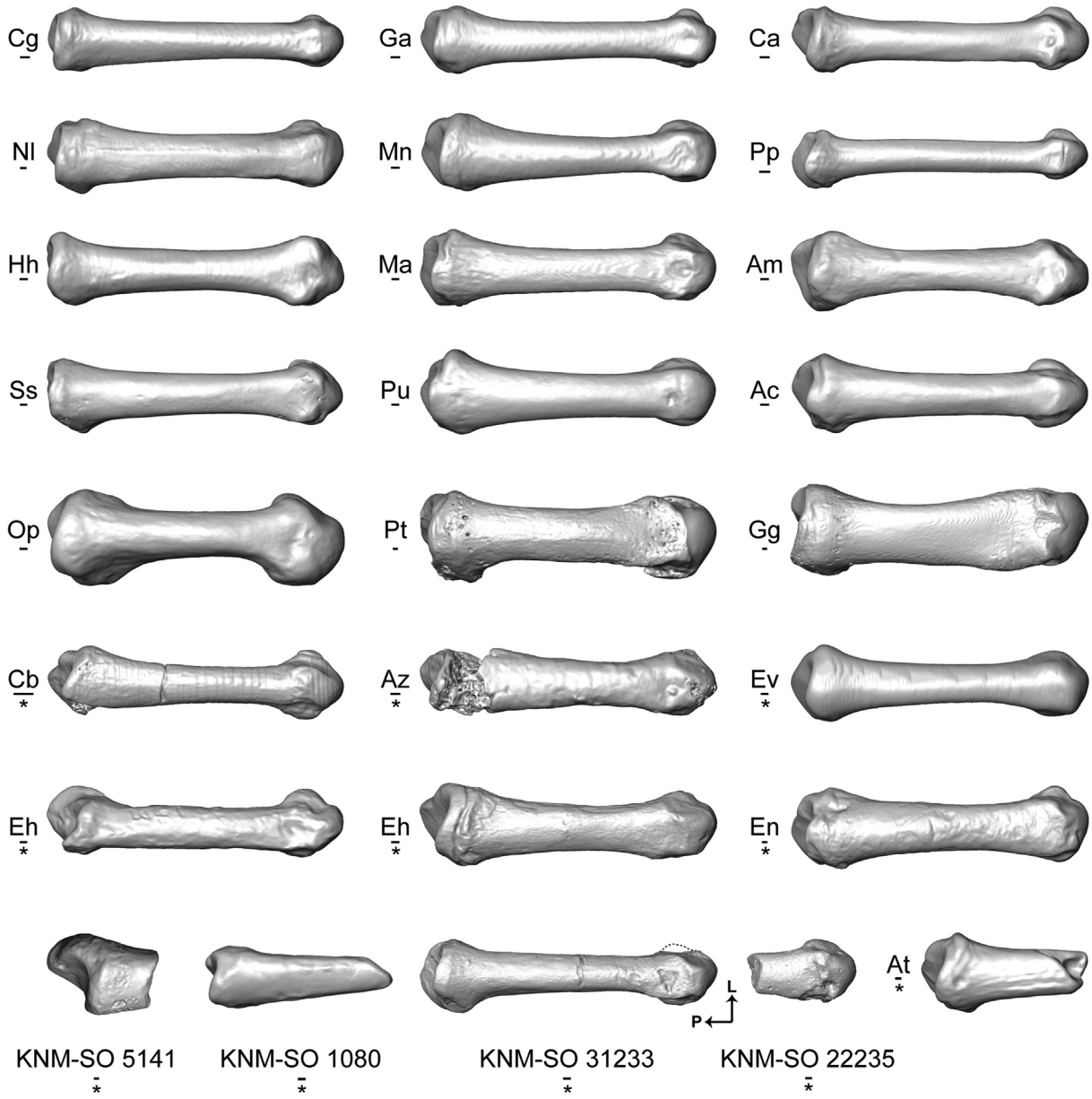


**Figure 4.** Representative virtual reconstructions of extant and fossil Mt1s in dorsal view (with respect to the bone's distal end). The fossils specimens are indicated by an asterisk (*). All specimens are originally from the left side except the following which have been mirror-imaged: KNM-RU 2036; KNM-KPS III; KNM-WK 18119; KNM-SO 22235. Lateral is to the top and proximal is to the left. Taxonomic abbreviations: Ac, *Alouatta caraya*; Am, *Ateles marginatus*; At, *Afropithecus turkanensis* (KNM-WK 18119); Az; *Aegyptopithecus zeuxis* (DPC 13318); Ca, *Cebus albifrons*; Cb; *Catopithecus browni* (DPC 20939); Cg, *Colobus guereza*; Ev, *Epipliopithecus vindobonensis* (Ind. 3); Eh, *Ekembo heseloni* (KNM-KPS III is on the left and KNM-RU 2036 is in the center); En, *Ekembo nyanzae* (KNM-RU 5872); Ga, *Cercopithecus ascanius*; Gg, *Gorilla gorilla*; Hh, *Hoolock hoolock*; Ma; *Cercocebus galeritus*; Mn, *Macaca nemestrina*; Nl, *Nasalis larvatus*; Op, *Pongo pygmaeus*; Pp, *Pithecia pithecia*; Pt, *Pan troglodytes*; Pu, *Papio ursinus*; Ss, *Symphalangus syndactylus*. Dotted lines on the distal end of specimen KNM-SO 31233 represent a reconstructed lateral epicondyle. Scale bars below species/specimen number equal 1 mm. See Appendix for ID numbers of extant specimens.

In most extant anthropoids except *Alouatta*, some atelines and some cercopithecines, the proximal base is taller than it is wide (see also Harrison, 1982). KNM-SO 31233, but not KNM-SO 1080 and 5141, has a relatively wider than tall proximal base, and overlaps the morphology exhibited by many specimens of *Alouatta*, *Ateles*, *Lagothrix*, *Lophocebus* and *Cercopithecus* (Fig. 6F). Base shape in the other fossil catarrhines is highly variable and without distinct patterns (see Index 6 in Table 3). The base in all three of these Songhor specimens shows evidence for a facet for the prehallux. This feature is visible in other known fossil catarrhine Mt1s from the Paleogene including *Catopithecus* (DPC 20939, Patel et al., 2012) and *Aegyptopithecus* (DPC 13318, Patel et al., 2012; YPM 25806, Conroy, 1976), as well as from the early Miocene *E. heseloni* (KNM-RU 2036, Lewis, 1972; KNM-KPS VIII, observed in this study) and *E. nyanzae* (KNM-RU 5872 and 17392, observed in this study). According to Ishida et al. (2004), the Mt1 of *N. kerioi* (KNM-BG 35250AJ) lacks a distinct facet for a prehallux; we were unable to verify this on our own cast of the specimen. Like many anthropoids, and the other fossil catarrhines studied here, KNM-SO 1080 has a distinct lateroplantar notch on the proximal articular surface (Fig. 5), but this feature is muted in KNM-SO 31233 and is absent in KNM-SO 5141. All three of these Songhor Mt1s are like most anthropoids and other fossil catarrhine Mt1s in having proximal articular surfaces with a greater concavity from medial to lateral, but a relatively flat surface from dorsal to plantar. That is to say they are not truly

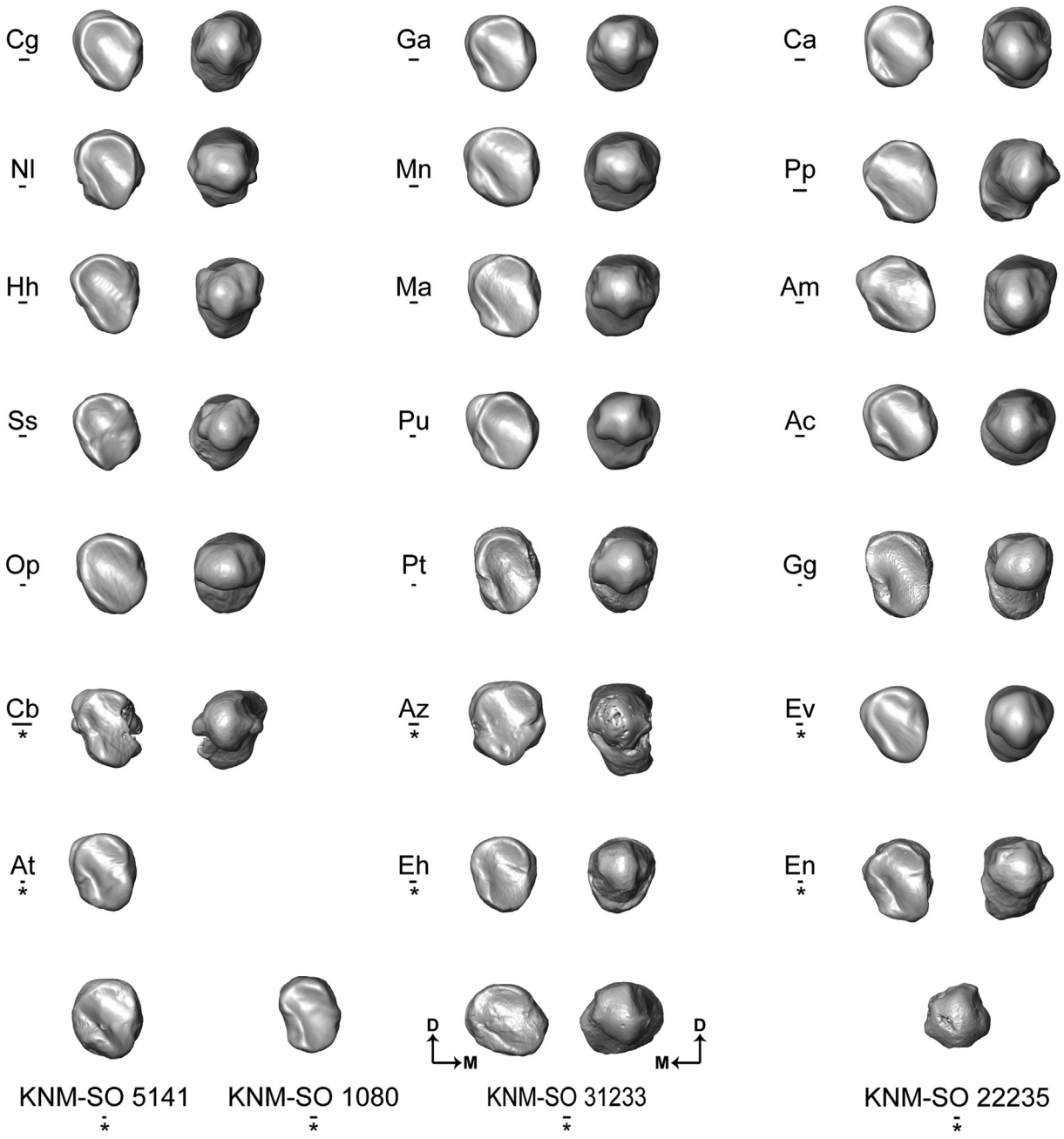


**Figure 5.** Representative virtual reconstructions of extant and fossil Mt1s in proximal (left) and distal (right) views. The fossils specimens are indicated by an asterisk (*). All specimens are originally from the left side except the following which have been mirror-imaged: KNM-RU 2036; KNM-WK 18119; KNM-SO 22235. Dorsal is to the top in both views; medial is to the right in proximal view and to the left in distal view. Taxonomic abbreviations: Ac, *Alouatta caraya*; Am, *Ateles marginatus*; At, *Afropithecus turkanensis* (KNM-WK 18119); Az; *Aegyptopithecus zeuxis* (DPC 13318 for the distal view; YPM 25806 for the proximal view); Ca, *Cebus albifrons*; Cb; *Catopithecus browni* (DPC 20939); Cg, *Colobus guereza*; Ev, *Epipliopithecus vindobonensis* (Ind. 3); Eh, *Ekembo heseloni* (KNM-RU 2036); En, *Ekembo nyanzae* (KNM-RU 5872); Ga, *Cercopithecus ascanius*; Gg, *Gorilla gorilla*; Hh, *Hoolock hoolock*; Ma; *Cercocebus galeritus*; Mn, *Macaca nemestrina*; Nl, *Nasalis larvatus*; Op, *Pongo pygmaeus*; Pp, *Pithecia pithecia*; Pt, *Pan troglodytes*; Pu, *Papio ursinus*; Ss, *Symphalangus syndactylus*. Scale bars below species/specimen number equal 1 mm. See Appendix for ID numbers of extant specimens.

saddle-shaped as in strepsirrhines and tarsiers (Szalay and Dagosto, 1988).

There is a great deal of overlap in Mt1 shaft torsion among anthropoids (Goodenberger et al., 2015). Although this was not quantified here, KNM-SO 31233 displays more torsion than most other extant anthropoids. Hallucal metatarsal torsion, however, does not appear to be like that of many strepsirrhines and does not approach the morphology seen in lorises. Similarly, although PAA has been shown to distinguish strepsirrhines and anthropoids well, the latter group has a very large range of overlap (Table 1; see also Goodenberger et al., 2015). KNM-SO 31233 has a PAA value (Table 2) that is in the higher range of most monkeys, above that of extant hominoids, at the lower range of platyrrhines, and overlaps with other fossil catarrhines in which this variable could be measured or estimated (Table 1). In contrast, the estimated PAA value for the very fragmentary KNM-SO 5141 is the highest among the entire sample. This is likely due to the fact that the proximal end of the bone is very asymmetric across the medial and lateral sides (Fig. 4). It is important to note, however, that without the entire shaft present, PAA values for fragmentary specimens should be treated with caution. Additionally, the full range of variation in extant anthropoid groups is not entirely known because of small sample

**Table 3**
Mt1 indices for fossil specimens.[a]

| Fossil – Taxon | Index 1[c] | Index 2[d] | Index 3[e] | Index 4[f] | Index 5[g] | Index 6[h] |
|---|---|---|---|---|---|---|
| KNM-SO 31233 | 5.49 | 12.46 | 85.52 | 66.93 | 86.53 | 91.32 |
| KNM-SO 1080 | – | – | 73.02 | – | – | 120.88 |
| KNM-SO 5129[b] | – | – | – | – | – | – |
| KNM-SO 5141 | – | – | – | – | – | 117.71 |
| KNM-SO 22235 | – | – | – | 62.50 | 91.35 | – |
| DPC 13318 – *Aegyptopithecus zeuxis* | 4.55 | 16.73 | 77.74 | 81.99 | 94.05 | 141.48 |
| YPM 25806 – *Aegyptopithecus zeuxis* | – | – | – | – | – | 107.01 |
| DPC 20939 – *Catopithecus browni* | 6.00 | 13.32 | 78.33 | 57.22 | 73.33 | 121.73 |
| *Epipliopithecus vindobonensis* (Individual 1) | 4.89 | 14.65 | 88.18 | 69.35 | 97.01 | 107.51 |
| *Epipliopithecus vindobonensis* (Individual 2) | 4.93 | 13.78 | 86.50 | 66.97 | 101.24 | 109.04 |
| *Epipliopithecus vindobonensis* (Individual 3) | 4.98 | 13.95 | 87.50 | 67.19 | 100.00 | 111.74 |
| KNM-CA 1865 – *Proconsul* cf. *africanus* | – | – | – | – | – | 111.88 |
| KNM-CA 1889 – *Proconsul* cf. *africanus* | – | – | – | – | 93.88 | – |
| KNM CA 2236 – *Proconsul* cf. *africanus* | – | – | – | – | 89.41 | – |
| KNM-CA 2239 – *Proconsul* cf. *africanus* | – | – | – | – | 86.73 | – |
| KNM-KPS III – *Ekembo heseloni* | – | 15.54 | 98.98 | 65.53 | 93.48 | – |
| KNM-KPS VIII – *Ekembo heseloni* | – | – | – | – | 82.35 | – |
| KNM-RU 15074 – *Ekembo heseloni*[†] | – | – | – | 65.50 | 86.70 | – |
| KNM-RU 17392 – *Ekembo nyanzae* | 4.76 | 16.58 | 82.55 | 71.05 | 92.11 | 120.95 |
| KNM-RU 2036 – *Ekembo heseloni* | 4.06 | 16.82 | 82.79 | 84.80 | 86.46 | 101.87 |
| KNM-RU 5872 – *Ekembo nyanzae* | 4.52 | 16.83 | 85.60 | 68.65 | 83.28 | 114.81 |
| KNM-WK 18119 – *Afropithecus turkanensis* | – | – | – | – | – | 126.79 |
| KNM-BG 17814 – *Nacholapithecus kerioi*[†] | – | – | – | 58.80 | 84.20 | – |
| GSP 14046 – *Sivapithecus parvada* | – | – | – | 62.20 | 90.80 | – |

[a] Indices derived from raw data presented in Table 2 except for those marked with [†] which are from Rose et al. (1996). Data for the extant sample are shown in Figure 6. Abbreviations in Index definitions are provided in the text and Table 1.
[b] Indices were not available for this specimen because of incomplete preservation of relevant variables.
[c] Index 1, relative length = IAL/sqrt CunM Area.
[d] Index 2, relative midshaft robusticity = ((50%-DPH × 50%-MLW)/2)/IAL) × 100.
[e] Index 3, relative proximodistal shaft width tapering = (75%-MLW/25%-MLW) × 100.
[f] Index 4, relative distal shaft to head shaft width = (75%-MLW/H-MLW) × 100.
[g] Index 5, head shape = (H-DPH/H-MLW) × 100.
[h] Index 6, base shape = (B-DPH/B-MLW) × 100.

sizes in previous studies (Jacobs et al., 2009; Patel et al., 2012; Goodenberger et al., 2015).

Qualitatively and quantitatively, KNM-SO 31233 has mixed morphology with its overall appearance resembling different aspects of the following extant primates: *Pithecia*, *Ateles*, *Colobus*, *Cercopithecus* and *Hylobates*. Its absolute length is similar to female *Ateles* and *Hylobates*. Its proximal articular surface area is similar to male *Macaca mulatta* and female *Nasalis* and *Hylobates*. Its overall size and shape (assessed using a geometric mean of 11 variables; Tables 1 and 2) are similar to several species of *Macaca*, *Ateles* and *Hylobates*. In general, KNM-SO 31233 looks very different from all other Paleogene and early Miocene catarrhine Mt1s for which comparisons can be made. It is not possible to say with any certainty which extant anthropoids KNM-SO 1080, 5129, 5041 and 22235 resemble the most because of their fragmentary preservation.

The anatomical descriptions and comparisons presented above indicate that the Songhor fossil Mt1s represent multiple size and shape morphs. Moreover, they cannot be confidently distinguished as extant hominid-, hylobatid-, cercopithecoid- or platyrrhine-like in their total morphological patterns.

### 3.3. Multivariate analysis of Mt1 shape

The PCA resulted in a total of 11 principal components (PC) with 65.11% of the total variation accounted for by the first two PCs (Table 4). Graphical ordination of PC1 and PC2 scores of the extant sample clearly results in two, albeit large, morphospaces – one for great apes and the other for monkeys and hylobatids (Fig. 7). PC1 describes 43.53% of the total variation and separates individual specimens such that positive values are correlated with relatively taller (DPH) and wider (MLW) shaft dimensions (at 25–75% of diaphyseal length) and relatively taller proximal bases (B-DPH) (Table 4). Despite the great deal of overlap on PC1 between taxonomic groups, most of the hylobatids, African colobines, arboreal guenons, atelines, and pithecids occupy the negative morphospace (Fig. 7; see SOM Table S6). PC2 accounts for 21.58% of the total variation and separates individual specimens in the positive direction based on relatively longer lengths (IAL), taller and wider heads (H-DPH, H-MLW), and a relatively wide base (B-MLW). Specimens in the negative direction on PC2 are further separated by having relatively tall and relatively wide shafts at 25% of diaphyseal length and 75% of diaphyseal length (25%-DPH and 75%-MLW) respectively. Greats apes, some hylobatid specimens, and several of the more terrestrial Old World monkey species separate into the negative morphospace along PC2 (Fig. 7, see SOM Table S6).

In accordance with the univariate analyses presented above, KNM-SO 31233 falls within the same morphospace as most hylobatids, arboreal guenons, capuchins, pithecids, and atelines (Fig. 7). The three specimens that are closest to it are those belonging to *Hylobates*, *Symphalangus* and *Sapajus* (SOM Table S6). Except for the *C. browni* Mt1, KNM-SO 31233 is the fossil Mt1 furthest removed from the extant great ape morphospace. In contrast, specimens belonging to *E. heseloni*, *E. nyanzae*, and *A. zeuxis* straddle a position in between great apes and the rest of the monkey and hylobatid sample, but there is some overlap with hylobatids. Only *E. nyanzae* comes close to the *Alouatta* shape space. *Epipliopithecus* specimens occupy a more central position relative to the entire extant sample, but they too are far from extant great apes. Of all the fossil Mt1s examined in this analysis, only those attributed to *Epipliopithecus* are within the *Alouatta* morphospace.

### 3.4. Taxonomic assessment from molar size predictions

Predicted values of $M_2$ MDL from Mt1 size variables for KNM-SO 5141, 1080, 22235 and 31233 are illustrated in Figure 8. Despite

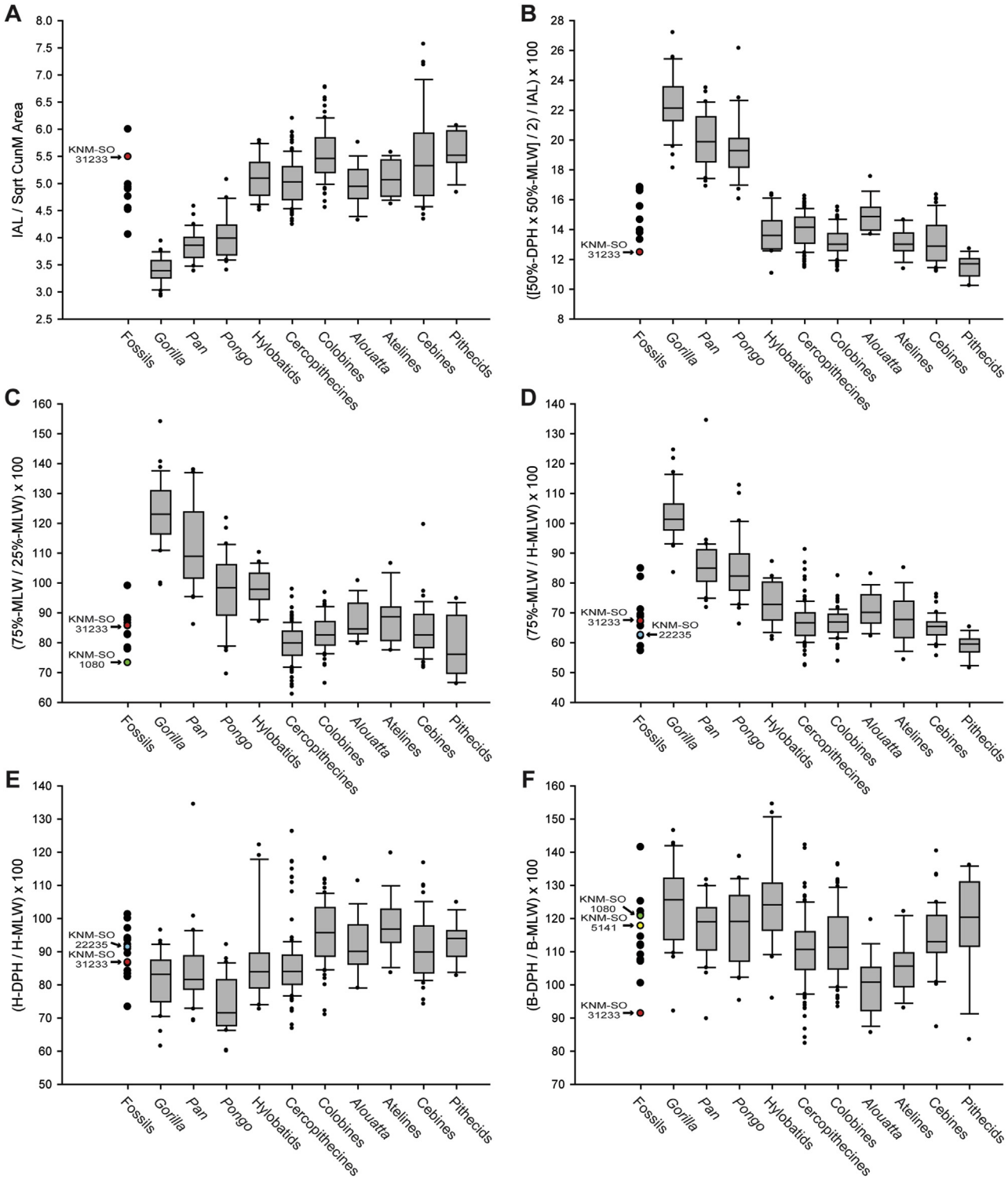


**Figure 6.** Box-and-whiskers plots: (A) relative length index: IAL divided by the square-root of the CunM Area; (B) midshaft robusticity index: the average of 50%-DPH and 50%-MLW divided by IAL; (C) proximodistal shaft tapering index: 75%-MLW divided by 25%-MLW; (D) distal shaft to head expansion index: 75%-MLW divided by H-MLW; (E) head shape index: H-DPH divided by H-MLW; (F) base shape index: B-DPH divided by B-MLW. Horizontal lines within each box illustrate the median of the distribution. Boxes envelop the interquartile range (50% of values) of the sample distribution, and whiskers encompass the range excluding outliers. Filled circles beyond whiskers indicate outliers. For the fossils, only the Songhor Mt1s are highlighted; data for the other fossils are found in Table 3. Extant group compositions based on species and specimens in Table 1.

relatively large prediction intervals for all comparisons, the following assessments can be made. Using CunM Area, KNM-SO 5141 can be attributed to *P. major*. For KNM-SO 1080, predictions of $M_2$ MDL also based on CunM Area fall inconclusively between the ranges of the larger *Rangwapithecus* and smaller *Dendropithecus* or *Limnopithecus*. In contrast, predictions based on CunM Area for KNM-SO 31233 suggest that this specimen can be allocated to either *Dendropithecus* or *Limnopithecus*. Using GMean(11) to predict $M_2$ MDL also positions KNM-SO 31233 in the upper range of the *Limnopithecus* and lower range of *Dendropithecus* $M_2$ MDL. Also, the

**Table 4**
Results for the principal components analysis (PCA) based on 11 Mt1 variables.[a]

| Variable[b] | PC 1 | PC 2 | PC 3 | PC 4 | PC 5 | PC 6 | PC 7 | PC 8 | PC 9 | PC 10 | PC 11 |
|---|---|---|---|---|---|---|---|---|---|---|---|
| LN IAL | −0.077 | 0.589 | 0.126 | −0.187 | 0.172 | −0.028 | 0.198 | −0.033 | −0.234 | 0.683 | 0.069 |
| LN B-DPH | 0.321 | 0.011 | 0.479 | −0.478 | −0.006 | 0.092 | 0.508 | 0.111 | −0.124 | −0.377 | 0.051 |
| LN B-MLW | 0.242 | 0.326 | −0.385 | 0.483 | −0.023 | −0.183 | 0.592 | 0.108 | 0.175 | −0.159 | 0.004 |
| LN 25%-DPH | 0.360 | −0.286 | 0.084 | 0.016 | 0.059 | 0.308 | 0.186 | −0.344 | 0.464 | 0.403 | −0.391 |
| LN 25%-MLW | 0.293 | 0.154 | −0.577 | −0.306 | −0.034 | 0.438 | −0.106 | −0.368 | −0.206 | −0.133 | 0.252 |
| LN 50%-DPH | 0.363 | 0.051 | 0.164 | 0.032 | 0.521 | −0.446 | −0.247 | −0.308 | 0.223 | −0.081 | 0.395 |
| LN 50%-MLW | 0.381 | 0.058 | −0.229 | −0.158 | 0.390 | −0.047 | −0.265 | 0.545 | −0.130 | −0.001 | −0.486 |
| LN 75%-DPH | 0.367 | −0.046 | 0.251 | 0.457 | −0.175 | −0.043 | −0.105 | −0.274 | −0.659 | 0.013 | −0.194 |
| LN 75%-MLW | 0.358 | −0.305 | 0.009 | 0.119 | −0.221 | 0.131 | −0.031 | 0.485 | 0.000 | 0.371 | 0.570 |
| LN H-DPH | 0.054 | 0.505 | 0.351 | 0.300 | 0.004 | 0.543 | −0.310 | 0.140 | 0.275 | −0.204 | 0.042 |
| LN H-MLW | 0.271 | 0.291 | 0.006 | −0.265 | −0.680 | −0.394 | −0.259 | −0.034 | 0.253 | 0.035 | −0.141 |
| Eigenvalue | 4.788 | 2.373 | 0.956 | 0.686 | 0.612 | 0.465 | 0.384 | 0.270 | 0.226 | 0.133 | 0.106 |
| % variance | 43.53 | 21.58 | 8.69 | 6.24 | 5.56 | 4.22 | 3.49 | 2.46 | 2.06 | 1.21 | 0.97 |

[a] Loadings for each variable on each principal component (PC).
[b] LN, natural log; IAL, interarticular length; DPH, dorsoplantar height, MLW, mediolateral width; B, base; H, head; 25%, 25% of shaft length from the proximal end; 50%, midshaft; 75%, 75% of shaft length from the proximal end.

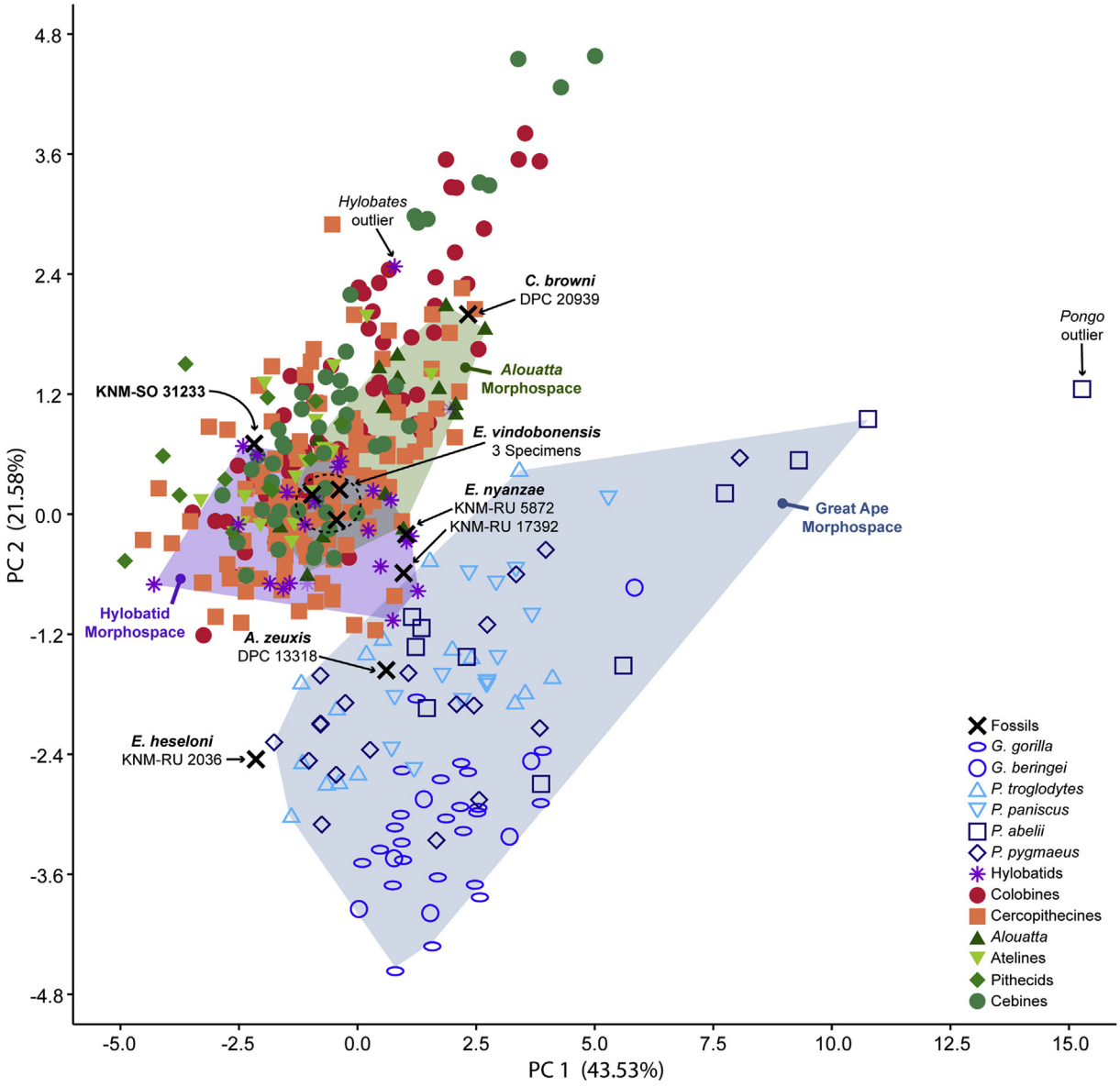


**Figure 7.** Principal components analysis (PCA) of 11 Mt1 scaled linear variables. The first two principal components (PC) accounting for 65.11% of the total variance are illustrated. Table 4 provides details about PC loadings. Extant great apes are in open blue-shaded symbols. Hylobatids are represented by purple asterisks (*). Cercopithecoids are in red-shaded closed symbols. Platyrrhines are in green-shaded closed symbols. Fossils are indicated by an **X**. The morphospaces for great apes, hylobatids and *Alouatta* are identified. A single *Hylobates* specimen and a single *Pongo* specimen were outliers and not included in their respective morphospace polygons. Note one distinct cluster for great apes and another for hylobatids and monkeys. KNM-SO 31233 is on the periphery of the hylobatid morphospace and within the monkey cluster, but is outside the *Alouatta* morphospace. It falls closest to specimens belonging to *Hylobates*, *Pithecia*, *Ateles*, *Colobus* and *Cercopithecus*. See SOM Table S6 for resulting PC scores for each specimen in the analysis. (For interpretation of the references to color in this figure legend, the reader is referred to the web version of this article.)

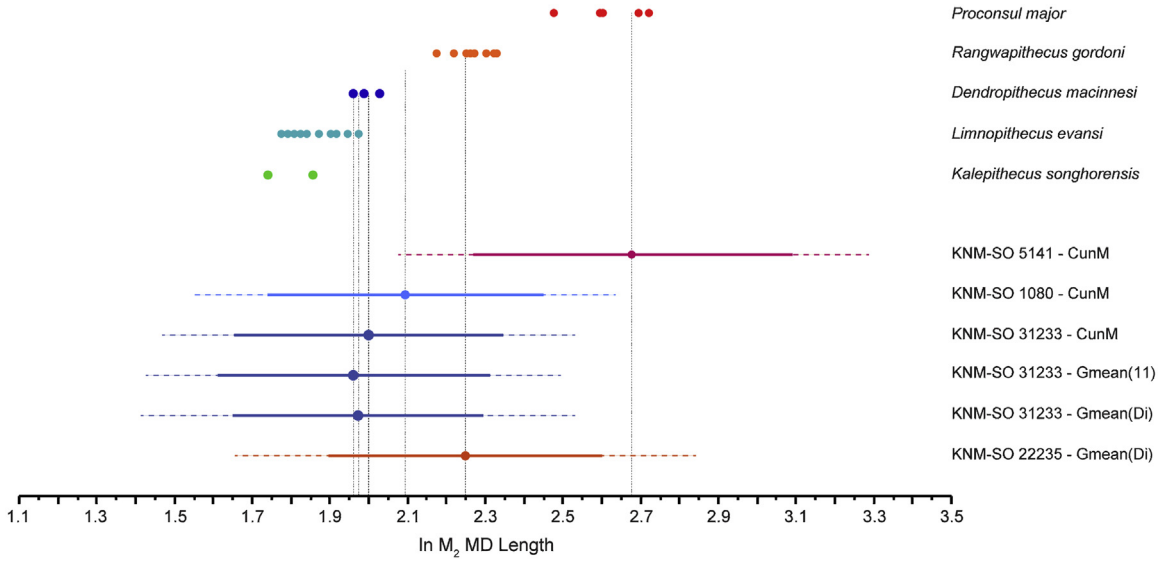


**Figure 8.** Lower second molar ($M_2$) mesiodistal length (MDL) predictions generated from least-squares regressions on three Mt1 size variables: CunM, GMean(11), and GMean(Di). The top portion of the figure illustrates known $M_2$-MDL dimensions for the five catarrhine primates found at Songhor (see SOM Table S4). The bottom portion of the figure shows predicted $M_2$-MDL values from four Songhor Mt1s described in this study. The solid circles are predicted values, with 95% confidence intervals and 95% prediction intervals shown in solid and broken lines, respectively. KNM-SO 5141 is confidently attributed to *Proconsul major*. KNM-SO 22235 is also confidently attributed to *Rangwapithecus gordoni*. KNM-SO 31233 can be attributed to either *Limnopithecus evansi* or *Dendropithecu macinnesi*, although the latter is preferred based on analyses of body mass predictions. KNM-SO 1080 is difficult to classify as either *D. macinnesi* or *R. gordoni*, although the latter is preferred based on analyses of body mass predictions. See text for additional details.

$M_2$ MDL predictions based on GMean(Di) for KNM-SO 31233 suggests that this specimen can be attributed to *Dendropithecus* or *Limnopithecus*. Therefore, using any of the three Mt1 size variables and despite large prediction intervals, KNM-SO 31233 can most likely be attributable to either *Dendropithecus* or *Limnopithecus*. Using GMean(Di) for KNM-SO 22235 indicates that this specimen may come from a larger animal that has lower molars the size of those of *Rangwapithecus*. Although KNM-SO 5129 was not included in this analysis, it likely would have fallen inconclusively between *Limnopithecus* or *Dendropithecus* and *Rangwapithecus*, similar to KNM-SO 1080, based on its H-DPH measurement (Table 2). In general, it is difficult to attribute any of these specimens to *Kalepithecus* (despite large overlapping statistical prediction intervals; Fig. 8) since it has some of the smallest known $M_2$s and because it is not very common at Songhor (as noted above).

### 3.5. Taxonomic assessment from body mass predictions

Regression equations and body mass predictions for specific fossils and fossil species means are presented in Tables 5 and 6, respectively. The predicted body mass for KNM-SO 5141 based on the square root of CunM Area is 65.79 kg. If this specimen is from *P. major* as suggested above, this value is within the range of previous predictions based on other postcranial remains for this species (63.4–86.7 kg; Rafferty et al., 1995). KNM-SO 5141 has a higher predicted mass than that for *E. nyanzae* and *A. turkanensis*, and of all the fossil Mt1s examined here, only the specimen for *S. parvada* yields a higher predicted mass (Table 6).

For KNM-SO 1080 the predicted body mass based on the square root of CunM Area is 11.86 kg. If this specimen represents *Dendropithecus* or *Limnopithecus*, it would exceed previous body mass predictions for both taxa (*Dendropithecus* range: 6.5–8.5 kg [Gingerich et al., 1982]; *Limnopithecus* range: 3.7–4.9 kg [Gingerich et al., 1982]) based on dental dimensions. Similarly, if this specimen represents *Rangwapithecus*, the predicted body mass would be on the lower end of the confidence interval derived from dental dimensions (11.4–15.2 kg [Gingerich et al., 1982]). According to our calculations, as well as from anatomical comparisons, we feel that attribution to *Rangwapithecus* is more parsimonious. The predicted mass for KNM-SO 1080 is much lower than mean values for *E. heseloni* Mt1s and fragmentary Mt1 specimens attributed to *P.* cf. *africanus* (Table 6).

The predicted body mass for KNM-SO 22235 based on two head dimensions is 22.25 kg. This value places this specimen well above the upper confidence interval for *Rangwapithecus*. But, without other possibilities (i.e., it being way too small to belong to *P. major*), *Rangwapithecus* is currently the most appropriate taxon to assign this specimen to. If both KNM-SO 22235 and 1080 belong to *Rangwapithecus*, the former may be from a male and the latter from a female considering that males of highly dimorphic catarrhines have larger Mt1 heads than females (Fig. 9). Although KNM-SO 5129 was not included in this analysis, based on its measurements of H-DPH, 75%-DPH and 75%-MLW (Table 2), it likely would have been slightly smaller than KNM-SO 22235, possibly also making this a large female or small male *Rangwapithecus*.

**Table 5**
Body mass prediction equations from Mt1 size variables.[a]

| Predictor[b] | *n*[c] | Slope | Slope 95% CI | Intercept | Intercept 95% CI | *p* | $r^2$ | MSE | %SEE | PRESS | QMLE |
|---|---|---|---|---|---|---|---|---|---|---|---|
| sqrt CunM Area | 111 | 0.905 | (0.845, 0.967) | −0.985 | (−1.101, −0.870) | <0.001 | 0.886 | 0.014 | 12.629 | 1.599 | 1.007 |
| GMean(11) | 111 | 0.898 | (0.857, 0.940) | −1.048 | (−1.127, −0.966) | <0.001 | 0.913 | 0.011 | 10.936 | 1.208 | 1.005 |
| sqrt Head Size | 111 | 0.957 | (0.903, 1.015) | −1.170 | (−1.278, −1.067) | <0.001 | 0.895 | 0.013 | 12.096 | 1.467 | 1.007 |

[a] *n*, sample size; CI, confidence interval; *p*, probability; $r^2$, coefficient of determination; MSE, mean square error; %SEE, percent standard error of the estimate; PRESS, predicted residual sum of squares; QMLE, quasi-maximum likelihood estimator.
[b] Variables defined in text.
[c] See SOM Table S6 for sample composition.

**Table 6**
Body mass predictions from metatarsal size variables.

| Taxon | Specimen/Mean[a] | sqrt CunM Area | | GMean(11) | | sqrt Head Size[b] | |
|---|---|---|---|---|---|---|---|
| | | Predicted BM (kg) | 95% PI (Lower, Upper) | Predicted BM (kg) | 95% PI (Lower, Upper) | Predicted BM (kg) | 95% PI (Lower, Upper) |
| | KNM-SO 31233 | 8.99 | (3.98, 20.30) | 7.73 | (3.80, 15.73) | 8.06 | (3.69, 17.61) |
| | KNM-SO 5141 | 65.79 | (28.72, 150.70) | – | – | – | – |
| | KNM-SO 1080 | 11.86 | (5.25, 26.79) | – | – | – | – |
| | KNM-SO 22235 | – | – | – | – | 22.25 | (10.14, 48.80) |
| *Aegyptopithecus zeuxis* | DPC 13318 | – | – | 7.56 | (3.72, 15.39) | 5.31 | (2.43, 11.60) |
| | Mean (n = 2) | 8.07 | (3.57, 18.22) | – | – | – | – |
| *Afropithecus turkanensis* | KNM-WK 18119 | 36.67 | (16.12, 83.41) | – | – | – | – |
| *Catopithecus browni* | DPC 20939 | 0.57 | (0.25, 1.32) | 0.79 | (0.38, 1.63) | 0.77 | (0.35, 1.72) |
| *Ekembo heseloni* | KNM-RU 2036 | 17.13 | (7.57, 38.75) | 13.41 | (6.58, 27.31) | – | – |
| | Mean (n = 3) | – | – | – | – | 14.54 | (6.64, 31.81) |
| *Ekembo nyanzae* | Mean (n = 2) | 38.65 | (16.98, 87.97) | 42.95 | (20.94, 88.12) | 45.12 | (20.43, 99.64) |
| *Epipliopithecus vindobonensis* | Mean (n = 3) | 14.02 | (6.20, 31.68) | 14.15 | (6.95, 28.82) | 15.84 | (7.23, 34.67) |
| *Proconsul* cf. *africanus* | Mean (n = 3) | – | – | – | – | 16.02 | (7.32, 35.06) |
| *Sivapithecus parvada* | GSP 14046 | – | – | – | – | 80.11 | (35.99, 178.34) |

[a] Mean predictions include all available specimens. When all available specimens do not preserve the necessary morphology, then predictions for individual specimens are reported [*Aegyptopithecus*: GMean(11), sqrt Head Size; *Ekembo heseloni*: sqrt CunM Area, sqrt GMean(11)].
[b] Head size = H-DPH × H-MLW.

For KNM-SO 31233 the predicted body masses have a mean range between 7.73 and 8.99 kg when considering all three Mt1 size variables. These values distinctively place this specimen within the confidence intervals of *Dendropithecus* (6.5–8.5 kg; Jungers, 1984) but above those of both *Limnopithecus* (3.7–4.9 kg; Gingerich et al., 1982) and *Kalepithecus* (4.5–6.1 kg; predicted from lower first molar equations in Gingerich et al. [1982] using specimens KNM-SO 378, KNM-CA 606, and KNM-CA 1778) body mass estimate ranges.

## 4. Discussion

The majority of the primate postcranial fossils from Songhor are fragmentary and there has been great difficulty in assigning these specimens to any of the five species of non-cercopithecoid catarrhines recognized there: *K. songhorensis*, *L. evansi*, *D. macinnesi*, *R. gordoni*, and *P. major* (Harrison, 1982; Langdon, 1986; Nengo and Rae, 1992; Gebo et al., 2009; Wurthrich et al., 2016). This places limits on the full understanding of the paleobiology of these taxa, especially with regards to reconstructing locomotor behavior and substrate preference. Moreover, because these species are diverse, especially in body size (e.g., Fleagle, 2013), an improved understanding of the Songhor postcranial material would shed light on the diversity and evolution of locomotor behaviors in Miocene catarrhines. This study focused on the hallucal metatarsal (Mt1) fossils that have been collected at Songhor since the 1960s.

### 4.1. Functional morphology

KNM-SO 31233 is the only complete Mt1 known from Songhor. Qualitative and quantitative analyses highlight the fact that its morphology resembles different aspects of several anthropoids including *Pithecia*, *Colobus*, *Cercopithecus*, *Ateles* and *Hylobates*. The Mt1 typical of these anthropoids are all relatively gracile and have a proximo-distally tapering diaphysis (Figs. 3–5). Gracile shafts suggest that substrate reaction forces acting on it during locomotion are probably not very high, and thus frequent bouts of forceful hallucal grasps may not be important. While it would be intriguing to conclude that KNM-SO 31233 came from an animal that was predominately suspensory because of its phenetic resemblance to *Hylobates* and *Ateles*, it is difficult to imagine how the morphology of a pedal element can be influenced solely by a forelimb-dominated behavior. However, because many non-siamang hylobatids engage in hindlimb leaping (e.g., Fleagle, 1976; Nowak and Reichard, 2016a, b), as do some pitheciines (Fleagle and Mittermeier, 1980), African colobines (e.g., Gebo and Chapman, 1995; McGraw, 1998; Stern and Goldstone, 2005) and guenons (e.g., Gebo and Chapman, 1995; McGraw, 1998; Stern and Goldstone, 2005), it is possible that the animal from which the KNM-SO 31233 Mt1 comes from was a frequent above-branch quadrupedal (or facultative bipedal) leaper. Anthropoids that frequently leap between higher and lower strata, or from one tree to another, may not need a robust Mt1 like typical arboreal quadrupeds that have to maintain long bouts of above-branch stability with great force (i.e., not frequently power-grasping; Patel et al., 2015). Similarly, it would not need a hyper-robust Mt1 as seen in strepsirrhines, many of which are grasp-leapers on narrow horizontal or vertical substrates (e.g., Szalay and Dagosto, 1988; Patel et al., 2012). Furthermore, it would not need a robust Mt1 that is characteristic of extant great apes that vertically climb large trunks or walk on the ground (Conroy and Rose, 1983). Therefore, if KNM-SO 31233 represents *Dendropithecus*, a conclusion supported by its predicted body mass and $M_2$ length (Fig. 8; Table 6), then interpretations of its morphology are consistent with those of other postcranial skeletal remains recognized from this species. Specifically, previous interpretations of *Dendropithecus* from Rusinga Island (and other small-bodied catarrhines like *Simiolus*), have promoted the possibility that it was adapted for above-branch quadrupedalism with frequent bouts of forelimb suspension and leaping (e.g., Le Gros Clark and Thomas, 1951; Harrison, 1982; Fleagle, 1983; Rose et al., 1992; Rose, 1993, 1996).

Additional evidence for correlating leaping with KNM-SO 31233 comes from the fact that its morphology is unlike *Alouatta* (Fig. 7). *Alouatta* is not usually regarded as a leaper and, in general, larger New World monkeys (including *Ateles*) leap with much less frequency (relative to smaller platyrrhines and colobine monkey; e.g., Fleagle and Mittermeier, 1980; Schön Ybarra, 1984; Youlatos, 2004; Nowak and Reichard, 2016a). Considering that the head size (= H-DPH x H-MLW) of KNM-SO 31233 was near half that of the *Epipliopithecus* Mt1s (resulting in a much smaller predicted body mass, Table 6), and that the latter had hindlimbs that were adapted for cautious, deliberate movements in the canopy without much leaping (Rose, 1993, 1996), it makes sense that only *Epipliopithecus* fossils were found in the *Alouatta* multivariate morphospace (Fig. 7). By extension, the Mt1s attributed to *Aegyptopithecus*, *Ekembo*, and other Miocene catarrhines suggest that they were also not very active leapers (e.g., Fleagle, 1983; Rose, 1996; Seiffert and Simons, 2001).

The preserved morphology of KNM-SO 1080 is similar to KNM-SO 31233 in some ways, especially with regards to a relatively gracile shaft that tapers from proximal to distal. Thus, it is possible

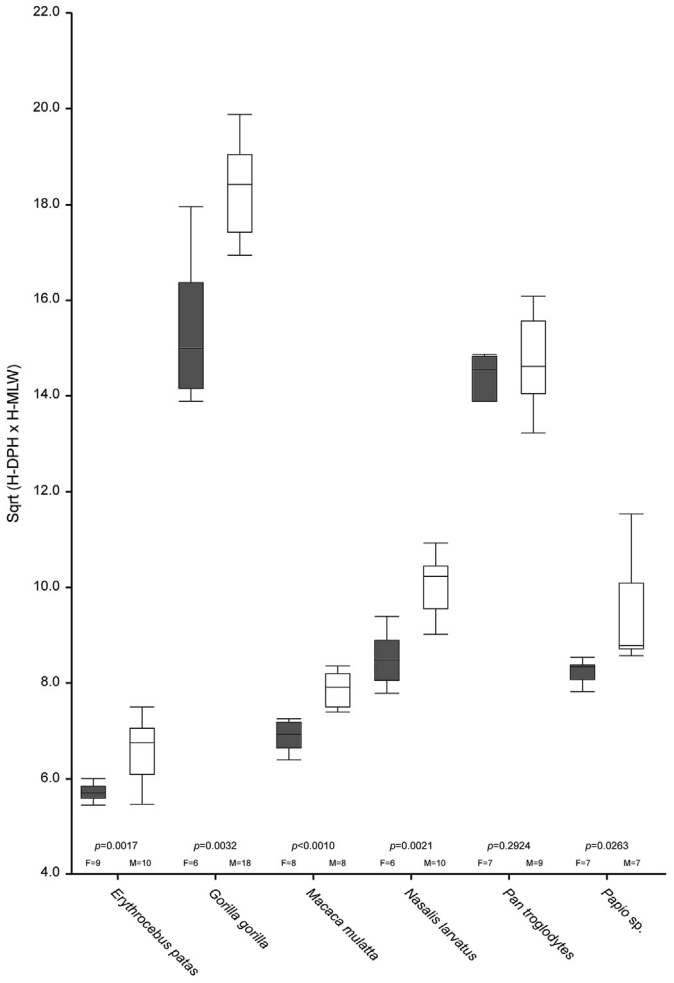


**Figure 9.** Box-and-whiskers plot of Mt1 head size (square root of H-DPH x H-MLW) in a sample of dimorphic catarrhines. Horizontal lines within each box illustrate the median of the distribution. Boxes envelop the interquartile range (50% of values) of the sample distribution, and whiskers encompass the range excluding outliers. Gray boxes are females and white boxes are males. Sample sizes for each sex-specific box and results of t-tests indicated at the bottom of the graph. Note that males tend to have larger Mt1 heads than females.

that it too may have used some leaping or simply did not rely on powerful hallucal grasping for postural and locomotor behaviors. One important difference between the two, however, is in their proximal articular surface morphology, which is deeper and mediolaterally compressed in the former (Figs. 1 and 5). In this regard, KNM-SO 1080 resembles other African Miocene taxa like *Ekembo*, *Afropithecus* and *Nacholapithecus*, as well as *Aegyptopithecus* from the Oligocene. In contrast to KNM-SO 31233, KNM-SO 1080 and other Miocene catarrhines may have had a slightly reduced range of motion in abduction-adduction at the entocuneiform-Mt1 joint and may have used arboreal supports with medium diameter sizes (relative to foot size) throughout the canopy.

Although predictions of $M_2$ length from Mt1 dimensions for KNM-SO 1080 are between *Rangwapithecus* and both *Dendropithecus* and *Limnopithecus* (Fig. 8), body mass predictions are confidently within the *Rangwapithecus* range. Therefore, we conclude that it is more parsimonious to suggest that KNM-SO 1080 belongs to *Rangwapithecus* and, by extension, its foot skeleton differed from *Dendropithecus*. While no postcranial specimens have yet to been confidently attributed to *Rangwapithecus*, a recent study of Songhor distal humeri allocated to this genus indicated that it was a generalized arboreal and climbing quadruped without any adaptations for suspension (Gebo et al., 2009), again making it different from *Dendropithecus*.

Relatively little can be said about the functional morphology of KNM-SO 5129 and 22235 (both attributed to *Rangwapithecus*) since they preserve only the head and distal end of the diaphysis. However, like other fossil catarrhines from the early Miocene (and possibly KNM-SO 31233), the preserved morphology of the distal end supports the hypothesis that it was likely capable of forceful flexion at the metatarsophalangeal joint. While the proximal end is not preserved, the distal morphology provides evidence that there was the ability to adduct at the entocuneiform-Mt1 joint. The lateral epicondyle is large (relative to the medial epicondyle) and this asymmetry is common in Miocene catarrhines (with preserved distal and proximal ends) as well as extant New World monkeys (Fig. 5). A large lateral epicondyle may increase the lever arm for the adductor hallucis muscle as its tendon crosses the MTP joint on its fibular side, thereby increasing the mechanical advantage of this main hallucal adductor. In contrast, extant apes have a relatively larger medial epicondyle (see above) which may suggest a greater emphasis on improving hallucal abduction efficiency as the tendon of the abductor hallucis muscle crosses the MTP joint capsule on its tibial side. Coupled with the fact that great apes, and to a lesser degree hylobatids, have large abductor hallucis muscles relative to total intrinsic foot musculature (Tuttle, 1972), greater mechanical advantage and more force can facilitate apes to abduct their hallux sufficiently and increase their pedal grip size to allow them to use large diameter horizontal branches, vertical tree trunks, or even the ground (e.g., Conroy and Rose, 1983). The medial epicondyle may also be large because deep to it would sit a sesamoid for the attachment of the medial head of the flexor hallucis brevis. In apes, this muscle, with the abductor hallucis, helps flex the MTP joint. In monkeys and Miocene catarrhines, it is likely that the adductor hallucis and the flexor hallucis brevis are more important for flexion and opposition.

While KNM-SO 5141 is fragmentary and preserves only its proximal end, the morphology seen is relatively unique for anthropoid primates. Unlike any other extant or fossil taxon, it is estimated that KNM-SO 5141 may have had a large physiological abduction angle and thus its foot would have had a prominent habitually abducted hallux. Along with a robust diaphysis (as estimated at the 75% position), this morphology could have aided not only in the habitual use of vertical climbing behaviors like those exhibited by extant great apes (Conroy and Rose, 1983), but also could have acted as a strut for supporting and stabilizing the medial side of the foot during terrestrial quadrupedal locomotion similar to that of African apes and possibly the earliest bipedal hominins (e.g., Vereecke et al., 2003; Lovejoy et al., 2009; Haile-Selassie et al., 2012). In fact, experimental studies have shown that when bonobos (*Pan paniscus*) walk quadrupedally on the ground, relative maximum plantar pressure values under the hallux are substantially higher in those individuals that have habitually more abducted big toes (see Table 4 in Vereecke et al., 2003). If the same hallucal loading patterns were experienced by the KNM-SO 5141 Mt1, and if this specimen is representative of *P. major* (according to predicted body mass and dental dimensions; see above), it would provide additional evidence that this large-bodied early Miocene catarrhine facultatively used terrestrial substrates (Harrison, 1982; Rafferty et al., 1995; Gommery et al., 1998, 2002).

### 4.2. The prehallux

The current study on early Miocene Mt1s provides a new opportunity to discuss the primate prehallux. The phylogenetic importance of a prehallux has been debated at length (Lewis, 1972; Wikander et al., 1986). According to Lewis (1972), among extant taxa

only hylobatids and platyrrhines have a prehallux, whereas cercopithecoids and hominoids (as well as strepsirrhines and tarsiers) lack this element. He hypothesized that this could suggest that stem-anthropoids had a prehallux that was then lost a number of times in catarrhine evolution including in cercopithecoids and extant great apes. Lewis (1972) supported this hypothesis in part by his observation (from casts) that *Dryopithecus africanus* (now *E. heseloni*) from Rusinga Island has a facet for a prehallux. He also suggested that because he saw no evidence of a prehallux facet in the Mt1s of *Pliopithecus vindobonensis* (now *E. vindobonensis*) - based on original drawings by Zapfe (1960) – this further demonstrated that the prehallux was lost a number of times in catarrhine evolution. Lewis (1972) also used this inference to argue that pliopithecoids had no phylogenetic relationship with living hylobatids since only the latter has a prehallux. With regards to extant forms, Wikander et al. (1986) generally agreed with this phylogenetic distribution, but also noted that the prehallux may not be homologous in hylobatids and platyrrhines, and that its variable presence within and between species in both appearance and development offers little resolution to the issue of character evolution.

The appearance of a prehallux pseudo-facet in many extant Mt1 specimens further complicates the issue. Wikander et al. (1986) demonstrated that in some species, such as *Pan troglodytes*, there are weak signs of a facet on the Mt1, which could be interpreted as an articulation for a prehallux, but their soft-tissue dissections showed no evidence of an actual sesamoid bone. They further noted that the presence of pseudo-facets could make fossil interpretations even more difficult. Despite this, it is interesting to note that among fossil catarrhines a prehallux facet or pseudo-facet appears to exist in the Paleogene species *C. browni* (Patel et al., 2012), *A. zeuxis* (Conroy, 1976; Patel et al., 2012) and the early Miocene species *E. heseloni* (Lewis, 1972; this study – visible on KNM-RU and KNM-KPS specimens), *E. nyanzae* (this study – visible on multiple KNM-RU specimens), *A. turkanensis* (this study – visible on KNM-WK 18119), *P. major* (this study – visible on KNM-SO 5141), *R. gordoni* (this study – visible on KNM-SO 1080), and *D. macinnesi* (this study – visible on KNM-SO 31233). Whether Miocene cercopithecoids had a prehallux is unknown, but it appears that among non-cercopithecoid catarrhines, the prehallux seems to have been lost, possibly independently, in the middle Miocene as evidenced by *E. vindobonensis* (Lewis, 1972) and *N. kerioi* (Ishida et al., 2004). Until a well-preserved articulated foot with all elements is found in the Miocene fossil record,[2] it is unlikely that the importance of the prehallux as a phylogenetically informative character will be resolved.

### 4.3. Evolution of primate hallucal grasping

The discovery of fossil Mt1s has significantly improved our understanding of the evolution of hallucal grasping in primates. For example, Mt1s from the Paleocene (attributed to plesiadapiforms) and from the Eocene (attributed to adapiforms, omomyiforms, and the stem-haplorhine *Eosimias*) have been fundamental in allowing researchers to understand key changes at the base of crown primates, including identifying hallucal synapomorphies of euprimates (e.g., Szalay and Dagosto, 1988; Bloch and Boyer, 2002; Gebo et al., 2008; Patel et al., 2012; Dunn et al., 2016). These include morphologies (e.g., a robust peroneal process, increased degree of physiological abduction, higher shaft torsion, a deep saddle-shaped proximal articular surface) related to powerful pedal grasping and for I–II and I–V grasp types that may have been necessary for utilizing relatively thin terminal branches or grasp-leaping positional behaviors in both horizontal and vertical orientations (e.g., Szalay and Dagosto, 1988; Goodenberger et al., 2015). Fossil Mt1s from the earliest stem-catarrhines of the Eocene and Oligocene of Africa (i.e., *Aegyptopithecus* and *Catopithecus*) have shown that the morphologies that characterize most extant anthropoids (e.g., small peroneal process, gracile shaft, decreased concavity of the proximal articular surface, reduced degree of physiological abduction), in contrast to those of extant strepsirrhines and tarsiers outlined above, are traits associated with increased reliance on quadrupedal locomotion on horizontal branches with large diameters (relative to body size) and are reversals and not primitive retentions from an ancestral primate condition (Conroy, 1976; Szalay and Dagosto, 1988; Patel et al., 2012). Hallucal metatarsals from the earliest hominins in the Pliocene (e.g., *Ardipithecus*) and those later in the Pleistocene (i.e., *Australopithecus*, early *Homo*) have revealed important changes in relative length, robusticity and degree of adduction of the big toe that have accompanied the evolution of bipedalism in the early part of the human career (e.g., Latimer et al., 1982; Susman and de Ruiter, 2004; Lovejoy et al., 2009; Pontzer et al., 2010; Haile-Selassie et al., 2012).

The present study on early Miocene catarrhine Mt1s from Songhor allows for a fresh look at and a better understanding of the morphological characters related to hallucal grasping and foot function in this group. Some Songhor catarrhines like *D. macinnesi* (based on an assignment for KNM-SO 31233) had an Mt1 with a diaphysis that was more gracile, exhibited more torsion, and with distal and proximal ends that highlight a greater need for hallucal adduction over abduction, albeit less forceful than contemporaneous Miocene taxa. Such a morphology is consistent with locomotor behaviors that relied on arboreal quadrupedalism and a large amount of leaping. Others like *P. major* (based on an assignment for KNM-SO 5141) appear to have a more robust hallux, possibly with a greater abducted orientation in its neutral position that might have facilitated vertical climbing on tree trunks, cautious above-branch movements, and terrestrial locomotion. This example of hallucal metatarsal diversity at Songhor and other contemporaneous localities in Kenya (with the presence of *Ekembo* and *Afropithecus*) and Eurasia (with *Epipliopithecus*) also demonstrates the diversity in the functional morphology of early catarrhine feet. Moreover, together they illustrate that not all early Miocene catarrhines were generalized, above-branch quadrupeds like many extant monkey species.

Considering that extant hylobatid Mt1s overlap significantly in the multivariate morphospace (Fig. 7) with both extant Old World and New World monkeys, and because they retain a prehallux like New World monkeys, it is possible that hylobatids retain a plesiomorphic Mt1 for anthropoids. In contrast, extant great apes are different from hylobatids and monkeys (e.g., Harrison, 1982; Conroy and Rose, 1983) by having Mt1s with a relatively short length, robust midshaft, minimally proximal-to-distal tapering shaft, a relatively large base and head, and larger medial than lateral distal epicondyles. With the growing number of fossil Mt1s from the Paleogene and Neogene (e.g., Conroy, 1976; Pilbeam et al., 1980; Harrison, 1982; Walker and Pickford, 1983; Rose et al., 1996; Ishida et al., 2004; Patel et al., 2012; this study), it is becoming clearer that the extant great ape morphology is derived (see Figs. 6 and 7). To test this hypothesis, however, proper comprehensive phylogenetic/character-based analyses are necessary (cf., Patel et al., 2012). When the extant great ape morphology appeared in the Miocene is also unclear since the only described middle Miocene specimens are also very fragmentary and/or have substantial taphonomic distortion (*Sivapithecus*: GSP 14046 [Pilbeam et al., 1980]; *Nacholapithecus*: KNM-BG 17814 and 35250AJ [Rose et al., 1996; Ishida et al., 2004]). Furthermore, we are unaware of any other described hallucal metatarsals from other later Miocene

[2] The Mt1 of the relatively well-preserved foot of *Oreopithecus bambolii* (specimen no. 36; Szalay and Langdon, 1986) is missing its proximal one-third.

hominoids like *Pierolapithecus* and *Hispanopithecus* that have relatively well-preserved postcranial skeletons (Alba, 2012). Therefore, when a more complete picture of early and middle Miocene hallux and foot function becomes available, this will undoubtedly shed light on the evolution of hallux function in the last common ancestors (LCA) of hominins and non-human apes (e.g., Lovejoy et al., 2009).

## 5. Conclusion

The early Miocene site of Songhor has yielded a large number of unassociated catarrhine postcranial remains from the hindlimb, including multiple elements from the foot. The primary goal of this study was to describe the hallucal metatarsal (Mt1) sample, which includes one complete specimen (KNM-SO 31233) and four fragmentary specimens (KNM-SO 1080, 5129, 5141, 22235). These fossils were compared to extant catarrhines and platyrrhines, as well as available fossil Miocene catarrhine Mt1s. Based on qualitative observations and quantitative analyses of size and shape, it is evident that the Songhor Mt1s are diverse, exhibiting a large robust morph (KNM-SO 5141) similar in size but not in shape to that of extant African apes, medium-sized morphs (KNM-SO 1080, 5129 and 22235), and a small slender one (KNM-SO 31233). The last is particularly interesting because its shape specifically resembles arboreal quadrupedal leaping monkeys and suspensory atelines and hylobatids, and this is unlike any other known fossil Miocene Mt1. Overall, however, none of the Songhor Mt1s resembled any one specific extant anthropoid clade or species since most non-great ape extant anthropoids overlap extensively in morphology. Additionally, none of these Miocene Mt1s has a morphology that is like extant great apes. This further emphasizes that the morpho-functional diversity of Songhor Mt1s is consistent with an extensive morphological and phylogenetic catarrhine diversity in the early part of the Miocene epoch.

## Author contributions

BAP and ION designed the study; BAP and CT collected the data; BAP and GSY analyzed the data; BAP drafted the manuscript; all authors gave final approval for publication.

## Acknowledgements

We thank Eileen Westwig and Neil Duncan from the AMNH, Nicole Edmison and Darrin Lunde from the USNM, Judy Chupasko from the MCZ, and Jim Dines from the LACM for their continued efforts in facilitating our research, including allowing frequent access to specimens in their care and the organization of specimen loans. Specimens housed in the RMCA were generously made available for study by Emannuel Gilissen. We also greatly appreciate the help of Terry Kensler and the Laboratory for Primate Morphology and Genetics of the CPRC for providing access to invaluable specimens in their care. The CPRC receives their funding from the National Institutes of Health (NIH 8 P40 OD012217-25). Rutger Jansma graciously shared results of his ongoing dissertation research on the reassessment of Miocene catarrhine teeth from Tinderet localities. Some of the fossil casts and/or 3D surface renderings of extant specimens were made available for this project by Holly Dunsworth, Masato Nakatsukasa, Erik Seiffert, Tea Jashashvili, Caley Orr, Mathew Tocheri, and Peter Fernandez. We also want to acknowledge the efforts of Benson Kyongo in making new fossil casts housed in the National Museums of Kenya. CT imaging played an important role in this study and we especially want to acknowledge the assistance from Tautis Skorka, Bino Varghese and Grant Dagliyan at the University of Southern California's Molecular Imaging Center, Stephan Judex at Stony Brook University, and the generous staff in the Department of Radiology at the Stony Brook University Medical Center. This paper benefited from conversations with Todd Rae and Erik Seiffert, as well as from valuable comments and editorial suggestions from the Associate Editor and our reviewers.

Generous financial support came from The Leakey Foundation (to BAP and ION), the National Science Foundation (grant numbers BSC-1317041 to BAP and BSC-1540421 to GSY and Doug Boyer), and the Core Fulbright Scholars Program, to ION. Additional funding was provided by the University of Southern California's URAP program (to BAP) and the University of Southern California's Office of the Provost (to CT).

## Appendix

| Specimen | Abbreviation in Figures 3–5 | Taxon | Morphosource specimen ID | DOI# |
|---|---|---|---|---|
| KNM SO 1080 | | cf *Rangwapithecus gordoni* | M13280-22968 | http://dx.doi.org/10.17602/M2/M22968 |
| KNM SO 22235 | | cf *Rangwapithecus gordoni* | M13281-22969 | http://dx.doi.org/10.17602/M2/M22969 |
| KNM SO 31233 | | cf *Dendropithecus macinnesi* | M13278-22966 | http://dx.doi.org/10.17602/M2/M22966 |
| KNM SO 5141 | | cf *Proconsul major* | M13279-22967 | http://dx.doi.org/10.17602/M2/M22967 |
| USNM 270355 | Ac | *Alouatta caraya* | M12811-21630 | http://dx.doi.org/10.17602/M2/M21630 |
| AMNH 95039 | Am | *Ateles marginatus* | M6866-7051 | http://dx.doi.org/10.17602/M2/M7051 |
| KNM WK 18119 | At | *Afropithecus turkanensis* | M13275-22963 | http://dx.doi.org/10.17602/M2/M22963 |
| DPC 13318 | Az | *Aegyptopithecus zeuxis* | M5142-4659 | http://dx.doi.org/10.17602/M2/M4659 |
| AMNH 188014 | Ca | *Cebus albifrons* | M13276-22964 | http://dx.doi.org/10.17602/M2/M22964 |
| DPC 20939 | Cb | *Catopithecus browni* | M5191-4700 | http://dx.doi.org/10.17602/M2/M4700 |
| AMNH 52229 | Cg | *Colobus guereza occidentalis* | M5238-4743 | http://dx.doi.org/10.17602/M2/M4743 |
| KNM KPS III | Eh | *Ekembo heseloni* | M13284-22972 | http://dx.doi.org/10.17602/M2/M22972 |
| KNM RU 2036 | Eh | *Ekembo heseloni* | M13285-22973 | http://dx.doi.org/10.17602/M2/M22973 |
| KNM RU 5872 | En | *Ekembo nyanzae* | M13286-22974 | http://dx.doi.org/10.17602/M2/M22974 |
| Individual 3 | Ev | *Epipliopithecus vindobonensis* | M13291-22979 | http://dx.doi.org/10.17602/M2/M22979 |
| AMNH 52554 | Ga | *Cercopithecus ascanius ascanius* | M13277-22965 | http://dx.doi.org/10.17602/M2/M22965 |
| AMNH 167335 | Gg | *Gorilla gorilla gorilla* | M13287-22975 | http://dx.doi.org/10.17602/M2/M22975 |
| AMNH 83425 | Hh | *Hoolock hoolock* | M13282-22970 | http://dx.doi.org/10.17602/M2/M22970 |
| AMNH 52641 | Ma | *Cercocebus galeritus agilis* | M5219-4725 | http://dx.doi.org/10.17602/M2/M4725 |
| AMNH 14012 | Mn | *Macaca nemestrina* | M5302-4807 | http://dx.doi.org/10.17602/M2/M4807 |
| AMNH 106272 | Nl | *Nasalis larvatus* | M13288-22976 | http://dx.doi.org/10.17602/M2/M22976 |
| AMNH 200900 | Op | *Pongo pygmaeus* | M5357-4857 | http://dx.doi.org/10.17602/M2/M4857 |
| AMNH 149149 | Pp | *Pithecia pithecia* | M5356-4856 | http://dx.doi.org/10.17602/M2/M4856 |
| AMNH 167342 | Pt | *Pan troglodytes* | M13283-22971 | http://dx.doi.org/10.17602/M2/M22971 |
| USNM 20860 | Pu | *Papio ursinus* | M13289-22977 | http://dx.doi.org/10.17602/M2/M22977 |
| USNM 271048 | Ss | *Symphalangus syndactylus* | M13290-22978 | http://dx.doi.org/10.17602/M2/M22978 |

## Supplementary Online Material

Supplementary online material related to this article can be found at http://dx.doi.org/10.1016/j.jhevol.2017.03.013.

## References


Alba, D.M., 2012. Fossil apes from the Vallès-Penedès Basin. Evol. Anthropol. 21, 254–269.

Andrews, P., 1978. A revision of the Miocene Hominoidea of East Africa. Bull. Br. Mus. Nat. Hist. (Geol.) 30, 85–224.

Bishop, W.W., Miller, J.A., Fitch, F.J., 1969. New potassium-argon age determinations relevant to the Miocene fossil mammal sequence in East Africa. Am. J. Sci. 267, 669–699.

Bloch, J.I., Boyer, D.M., 2002. Grasping primate origins. Science 298, 1606–1610.

Boyer, D.M., Patel, B.A., Larson, S.G., Stern Jr., J.T., 2007. Telemetered electromyography of peroneus longus in *Varecia variegata* and *Eulemur rubriventer*: implications for the functional significance of a large peroneal process. J. Hum. Evol. 53, 119–134.

Conroy, G.C., 1976. Hallucial tarsometatarsal joint in an Oligocene anthropoid *Aegyptopithecus zeuxis*. Nature 262, 684–686.

Conroy, G., Rose, M., 1983. The evolution of the primate foot from the earliest primates to the Miocene hominoids. Foot Ankle 3, 342–364.

Cote, S., Nengo, I.O., 2007. Inter- and intra-sexual dimorphism in an Early Miocene catarrhine - *Rangwapithecus gordoni* - as demonstrated by material from Western Kenya. Am. J. Phys. Anthropol S44, 91.

Cote, S., McNulty, K.P., Stevens, N.J., Nengo, I.O., 2016. A detailed assessment of the maxillary morphology of *Limnopithecus evansi* with implications for the taxonomy of the genus. J. Hum. Evol. 94, 83–91.

Dunn, R.H., Rose, K.D., Rana, R.S., Kumar, K., Sahni, A., Smith, T., 2016. New euprimate postcrania from the early Eocene of Gujarat, India, and the strepsirrhine-haplorhine divergence. J. Hum. Evol. 99, 25–51.

Fleagle, J.G., 1976. Locomotion and posture of the Malayan siamang and implications for hominoid evolution. Folia Primatol. 26, 245–269.

Fleagle, J.G., 1983. Locomotor adaptations of Oligocene and Miocene hominoids and their phyletic implications. In: Ciochon, R.L., Corruccinni, R.S. (Eds.), New Interpretations of Ape and Human Ancestry. Plenum Press, New York, pp. 301–324.

Fleagle, J.G., 2013. Primate Adaptation and Evolution, 3rd Edition. Academic Press, San Diego, CA.

Fleagle, J.G., Mittermeier, R.A., 1980. Locomotor behavior, body size, and comparative ecology of seven Surinam monkeys. Am. J. Phys. Anthropol. 52, 301–314.

Gebo, D.L., Chapman, C.A., 1995. Positional behavior in five sympatric Old World monkeys. Am. J. Phys. Anthropol. 97, 49–76.

Gebo, D.L., Dagosto, M., Beard, K.C., Ni, X., Qi, T., 2008. A haplorrhine first metatarsal from the Middle Eocene of China. In: Fleagle, J.G., Gilbert, C.C. (Eds.), Elwyn Simons: A Search for Origins. Springer, New York, pp. 229–242.

Gebo, D.L., Malit, N.R., Nengo, I.O., 2009. New proconsulid postcranials from the early Miocene of Kenya. Primates 50, 311–319.

Gingerich, P.D., Smith, B.H., Rosenberg, K., 1982. Allometric scaling in the dentition of primates and prediction of body weight from tooth size in fossils. Am. J. Phys. Anthropol. 58, 81–100.

Gommery, D., Senut, B., Pickford, M., 1998. Nouveaux restes postcrâniens d'Hominoidea du Miocène inférieur de Napak, Ouganda. Hommage à W.W. Bishop. Annales de Paléontologie 84, 287–306.

Gommery, D., Senut, B., Pickford, M., Musiime, E., 2002. Les nouveaux restes du squelette d'*Ugandapithecus major* (Miocène inférieur de Napak, Ouganda). Annales de Paléontologie 88, 167–186.

Goodenberger, K.E., Boyer, D.M., Orr, C.M., Jacobs, R.L., Femiani, J.C., Patel, B.A., 2015. Functional morphology of the hallucal metatarsal with implications for inferring grasping ability in extinct primates. Am. J. Phys. Anthropol. 156, 327–348.

Haile-Selassie, Y., Saylor, B.Z., Deino, A., Levin, N.E., Alene, M., Latimer, B.M., 2012. A new hominin foot from Ethiopia shows multiple Pliocene bipedal adaptations. Nature 483, 565–569.

Hammer, O., Harper, D.A.T., Ryan, P.D., 2001. PAST: Paleontological statistics software package for education and data analysis. Paleontol. Elec. 4, 1–9.

Harrison, T., 1982. Small-bodied apes from the Miocene of East Africa. Ph.D. Dissertation, University of London.

Harrison, T., 1988. A taxonomic revision of the small catarrhine primates from the Early Miocene of East Africa. Folia Primatol. 50, 59–108.

Harrison, T., 2002. Late Oligocene to middle Miocene catarrhines from Afro-Arabia. In: Hartwig, W.C. (Ed.), The Primate Fossil Record. Cambridge University Press, Cambridge, pp. 311–338.

Harrison, T., 2010. Dendropithecoidea, Proconsuloidea and Hominoidea. In: Werdelin, L., Sanders, W.J. (Eds.), Cenozoic Mammals of Africa. University of California Press, Berkeley, pp. 429–469.

Harrison, T., Andrews, P., 2009. The anatomy and systematic position of the early Miocene proconsulid from Meswa Bridge, Kenya. J. Hum. Evol. 56, 479–496.

Hill, A., Nengo, I.O., Rossie, J.B., 2013. A *Rangwapithecus gordoni* mandible from the early Miocene site of Songhor, Kenya. J. Hum. Evol. 65, 490–500.

Ishida, H., Kunimatsu, Y., Takano, T., Nakano, Y., Nakatsukasa, M., 2004. *Nacholapithecus* skeleton from the Middle Miocene of Kenya. J. Hum. Evol. 46, 69–103.

Isler, K., Kirk, E.C., Miller, J.M.A., Albrecht, G.A., Gelvin, B.R., Martin, R.D., 2008. Endocranial volumes of primate species: scaling analyses using a comprehensive and reliable data set. J. Hum. Evol. 55, 967–978.

Jacobs, R.L., Boyer, D.M., Patel, B.A., 2009. Comparative functional morphology of the primate peroneal process. J. Hum. Evol. 57, 721–731.

Jashashvili, T., Dowdeswell, M.R., Lebrun, R., Carlson, K.J., 2015. Cortical structure of hallucal metatarsals and locomotor adaptations in hominoids. PLOS ONE 10, e0117905.

Jungers, W.L., 1984. Aspects of size and scaling in primate biology with special reference to the locomotor skeleton. Am. J. Phys. Anthropol. 27, 73–97.

Jungers, W.L., Falsetti, A.B., Wall, C.E., 1995. Shape, relative size, and size-adjustments in morphometrics. Yearb. Phys. Anthropol. 38, 137–161.

Langdon, J.H., 1984. A comparative functional study of the Miocene hominoid foot remains. Ph.D. Dissertation, Yale University.

Langdon, J.H., 1986. Functional morphology of the Miocene hominoid foot. Contrib. Primatol. 22, 1–226.

Latimer, B.M., Lovejoy, C.O., Johanson, D.C., Coppens, Y., 1982. Hominid tarsal, metatarsal, and phalangeal bones recovered from the Hadar formation: 1974–1977 collections. Am. J. Phys. Anthropol. 57, 701–719.

Leakey, R.E., Leakey, M.G., Walker, A.C., 1988. Morphology of *Afropithecus turkanensis* from Kenya. Am. J. Phys. Anthropol. 76, 289–307.

Le Gros Clark, W.E., Thomas, D.P., 1951. Associated Jaws and Limb Bones of *Limnopithecus macinnesi*. Fossil Mammals of Africa, No. 3. British Museum (Natural History), London.

Lewis, O.J., 1972. The evolution of the hallucial tarsometatarsal joint in the Anthropoidea. Am. J. Phys. Anthropol. 37, 13–34.

Lewis, O.J., 1989. Functional Morphology of the Evolving Hand and Foot. Clarendon, Oxford.

Lovejoy, C.O., Latimer, B., Suwa, G., Asfaw, B., White, T.D., 2009. Combining prehension and propulsion: The foot of *Ardipithecus ramidus*. Science 326, 72.

MacInnes, D.G., 1943. Notes on the East African Miocene primates. J. E. Af. Nat. Hist. Soc. 17, 141–181.

MacLatchy, L., Rossie, J.B., 2005. The Napak hominoid: still *Proconsul major*. In: Lieberman, D.E., Smith, R.J., Kelley, J. (Eds.), Interpreting the Past: Essays on Human, Primate, and Mammal Evolution in Honor of David Pilbeam. Brill Academic Publishers, Boston, pp. 15–28.

Martin, R.D., 1990. Primate Origins and Evolution. Princeton University Press, Princeton.

McGraw, W.S., 1998. Comparative locomotion and habitat use of six monkeys in the Tai Forest, Ivory Coast. Am. J. Phys. Anthropol. 105, 493–510.

McNulty, K.P., Begun, D.R., Kelley, J., Manthi, F.K., Mbua, E.N., 2015. A systematic revision of *Proconsul* with the description of a new genus of early Miocene hominoid. J. Hum. Evol. 84, 42–61.

Meldrum, D.J., 1991. Kinematics of the cercopithecine foot on arboreal and terrestrial substrates with implications for the interpretation of hominid terrestrial adaptations. Am. J. Phys. Anthropol. 84, 273–289.

Morton, D.J., 1924. Evolution of the human foot II. Am. J. Phys. Anthropol. 7, 1–52.

Napier, J.R., Davis, P.R., 1959. The Fore-limb Skeleton and Associated Remains of *Proconsul africanus*. Fossil Mammals of Africa, No. 16. British Museum (Natural History), London.

Nengo, I.O., Rae, T.C., 1992. New hominid fossils from the early Miocene site of Songhor, Kenya. J. Hum. Evol. 23, 423–429.

Nowak, M.G., Reichard, U.H., 2016a. Locomotion and posture in ancestral hominoids prior to the split of hylobatids. In: Reichard, U.H., Hirai, H., Barelli, C. (Eds.), Evolution of Gibbons and Siamang: Phylogeny, Morphology, and Cognition. Springer, New York, pp. 55–89.

Nowak, M.G., Reichard, U.H., 2016b. The torso-orthograde positional behavior of wild white-handed gibbons (*Hylobates lar*). In: Reichard, U.H., Hirai, H., Barelli, C. (Eds.), Evolution of Gibbons and Siamang: Phylogeny, Morphology, and Cognition. Springer, New York, pp. 203–225.

Patel, B.A., Seiffert, E.R., Boyer, D.M., Jacobs, R.L., St. Clair, E.M., Simons, E.L., 2012. New primate first metatarsals from the Paleogene of Egypt and the origins of the anthropoid big toe. J. Hum. Evol. 63, 99–120.

Patel, B.A., Larson, S.G., Stern, J.T., 2015. Electromyography of crural and pedal muscles in tufted capuchin monkeys (*Sapajus apella*): Implications for hallucal grasping behavior and first metatarsal morphology in euprimates. Am. J. Phys. Anthropol. 156, 553–564.

Pickford, M., 1986. Cainozoic paleontological sites of Western Kenya. Münch. Geowissen. Abh. 8, 1–151.

Pickford, M., Andrews, P., 1981. The Tinderet Miocene sequence in Kenya. J. Hum. Evol. 10, 11–33.

Pickford, M., Senut, B., Gommery, D., Musiime, E., 2009. Distinctiveness of *Ugandapithecus* from *Proconsul*. Estudios Geologicos-Madrid 65, 183–241.

Pilbeam, D.R., Rose, M.D., Badgley, C., Lipschutz, B., 1980. Miocene hominoids from Pakistan. Postilla 181, 1–94.

Pontzer, H., Rolian, C., Rightmire, G.P., Jashashvili, T., Ponce de León, M.S., Lordkipanidze, D., Zollikofer, C.P.E., 2010. Locomotor anatomy and biomechanics of the Dmanisi hominins. J. Hum. Evol 58, 492–504.

Rafferty, K.L., Walker, A., Ruff, C., Rose, M.D., Andrews, P.J., 1995. Postcranial estimates of body weights in *Proconsul*, with a note on a distal tibia of *P. major* from Napak, Uganda. Am. J. Phys. Anthropol. 97, 391–402.

Rose, M.D., 1983. Miocene hominoid postcranial morphology. Monkey-like, ape-like, neither, or both? In: Ciochon, R.L., Corruccini, R.S. (Eds.), New Interpretations of Ape and Human Ancestry. Plenum Press, New York, pp. 405–417.

Rose, M.D., 1993. Locomotor antomy of Miocene hominoids. In: Gebo, D.L. (Ed.), Postcranial Adaptations in Non-human Primates. Northern Illinois University Press, Dekalb, pp. 252–272.
Rose, M.D., 1996. Functional morphological similarities in the locomotor skeleton of Miocene catarrhines and platyrrhine monkeys. Folia Primatol. 66, 7–14.
Rose, M.D., Leakey, M.G., Leakey, R.E.F., Walker, A., 1992. Postcranial specimens of *Simiolus enjiessi* and other primitive catarrhines from the early Miocene of Lake Turkana, Kenya. J. Hum. Evol. 22, 171–237.
Rose, M., Nakano, Y., Ishida, H., 1996. *Kenyapithecus* postcranial specimens from Nachola, Kenya. African Study Monographs 24, 3–56.
Schön Ybarra, M.A., 1984. Locomotion and postures of red howlers in a deciduous forest-savanna interface. Am. J. Phys. Anthropol. 63, 65–76.
Schultz, A.H., 1963. Relations between the lengths of the main parts of the foot skeleton in primates. Folia Primatol. 1, 150–171.
Seiffert, E.R., Simons, E.L., 2001. Astragalar morphology of late Eocene anthropoids from the Fayum Depression (Egypt) and the origin of catarrhine primates. J. Hum. Evol. 41, 577–606.
Senut, B., Pickford, M., Gommery, D., Kunimatsu, Y., 2000. Un nouveau genre d'hominoïde du Miocène inférieur d'Afrique orientale: *Ugandapithecus major* (Le Gros Clark and Leakey, 1950). C.R. Acad. Sci. Paris 331, 227–233.
Smith, F.A., Lyons, S.K., Ernest, S.K.M., Jones, K.E., Kaufman, D.M., Dayan, T., Marquet, P.A., Brown, J.H., Haskell, J.P., 2003. Body mass of late Quaternary mammals. Ecology 84, 3403–3403.
Smith, R.J., 1993. Bias in equations used to estimate primate body mass. J. Hum. Evol. 25, 31–41.
Smith, R.J., Jungers, W.L., 1997. Body mass in comparative primatology. J. Hum. Evol. 32, 523–599.
Sprugel, D.G., 1983. Correcting for bias in log-transformed allometric equations. Ecology 64, 209–210.
Stern, M., Goldstone, R., 2005. Red colobus as prey: the leaping habits of five sympatric Old World monkeys. Folia Primatol. 76, 100–112.
Susman, R.L., de Ruiter, D.J., 2004. New hominin first metatarsal (SK 1813) from Swartkrans. J. Hum. Evol. 47, 171–181.
Swindler, D.R., 2002. Primate Dentition: An Introduction to the Teeth of Non-Human Primates. Cambridge University Press, Cambridge.
Szalay, F.S., Dagosto, M., 1988. Evolution of hallucial grasping in the primates. J. Hum. Evol. 17, 1–33.
Szalay, F.S., Langdon, J.H., 1986. The foot of *Oreopithecus*: and evolutionary assessment. J. Hum. Evol. 15, 585–621.
Tuttle, R., 1972. Relative mass of cheiridial muscles in catarrhine primates. In: Tuttle, R. (Ed.), The Functional and Evolutionary Biology of Primates. Aldine-Atherton, Inc., Chicago, pp. 262–291.
Vereecke, E., D'Août, K., De Clercq, D., Van Elsacker, L., Aerts, P., 2003. Dynamic plantar pressure distribution during terrestrial locomotion of bonobos (*Pan paniscus*). Am. J. Phys. Anthropol. 120, 373–383.
Walker, A., Pickford, M., 1983. New postcranial fossils of *Proconsul africanus* and *Proconsul nyanzae*. In: Ciochon, R.L., Corruccinni, R.S. (Eds.), New Interpretations of Ape and Human Ancestry. Plenum Press, New York, pp. 325–351.
Walker, A., Teaford, M., 1988. The Kaswanga primate site: an early Miocene hominoid site on Rusinga Island, Kenya. J. Hum. Evol. 17, 539–544.
Wikander, R., Covert, H.H., DeBlieux, D.D., 1986. Ontogenetic, intraspecific, and interspecific variation of the prehallux in primates: implications for its utility in the assessment of phylogeny. Am. J. Phys. Anthropol. 70, 513–523.
Wurthrich, C., Orr, C.M., Patel, B.A., Nengo, I.O., 2016. Taxonomic affinities of catarrhine capitates from Songhor, early Miocene, Kenya. Am. J. Phys. Anthropol. S62, 339.
Yapuncich, G.S., 2017. Alternative methods for calculating percentage prediction error and their implications for predicting body mass in fossil taxa. J. Hum. Evol. http://dx.doi.org/10.1016/j.jhevol.2017.03.001.
Yapuncich, G.S., Gladman, J.T., Boyer, D.M., 2015. Predicting euarchontan body mass: A comparison of tarsal and dental variables. Am. J. Phys. Anthropol. 157, 472–506.
Youlatos, D., 2004. Multivariate analysis of organismal and habitat parameters in two Neotropical primate communities. Am. J. Phys. Anthropol. 123, 181–194.
Zapfe, H., 1958. The skeleton of *Pliopithecus (Epipliopithecus) vindobonensis* Zapfe and Hürzeler. Am. J. Phys. Anthropol. 16, 441–457.
Zapfe, H., 1960. Mit Anhang: Der Primatenfund aus dem Miozan uon Klein Hadersdorf in Niedenostemeich. Schweiz. Palaeontol. Die primatenfunde aus der Miozanen spaltenfullung von Neudorf an der March (Devinska Nova Ves), Tschechoslowakei, vol. 78, pp. l–293.
Zar, J.H., 1984. Biostatistical Analysis, 2nd Edition. Prentice-Hall, New Jersey.